

THESIS

316L STAINLESSS STEEL MODIFIED VIA PLASMA ELECTROLYTIC OXIDATION
FOR ORTHOPEDIC IMPLANTS

Submitted by

James A. Michael II

School of Biomedical Engineering

In partial fulfillment of the requirements

For the Degree of Master of Science

Colorado State University

Fort Collins, Colorado

Fall 2022

Master's Committee:

Advisor: Ketul C. Popat

Vivian Li

Walajabad S. Sampath

Copyright by James A. Michael II 2022

All Rights Reserved

ABSTRACT

316L STAINLESS STEEL MODIFIED VIA PLASMA ELECTROLYTIC OXIDATION FOR ORTHOPEDIC IMPLANTS

316L stainless steel (SS) is widely used biomaterial for implantable devices and is estimated to be the base material for 60% of implantable devices. However, one challenge of the material is the inhomogeneity of the surface morphology which may influence the adhesion process of host cells and bacteria. One method to create a uniform surface of 316L SS is plasma electrolytic oxidation (PEO). PEO creates an oxide layer on the outer surface thus changing the surface topography on the microscale. PEO process on SS functions by anodizing the surface via direct current in electrolyte solution. Preliminary research found that a continuous direct current over a time manufactured undesirable samples, to overcome this challenge the use of pulse timings was utilized during fabrication. This research aimed to answer the questions how do PEO modifications effect cellular adhesion and viability, and how do PEO modifications affect bacteria adhesion and viability. PEO modified 316L SS surfaces were characterized and its effects on the adhesion, morphology, and differentiation of adipocyte derived stem cells, along with the adhesion and morphology of *Staphylococcus aureus* was investigated.

ACKNOWLEDGEMENTS

I have many individuals to thank for helping me with completing this thesis. To my advisor Dr. Ketul Popat, thank you for the encouragement that you gave me. It got me to where I am now in my academic career. The talk you gave me, my first semester here at Colorado State University allowed me to persevere through this achievement.

I would like to thank Dr. Paulo Soares at the Pontifical Catholic University of Paraná in Curitiba, Brazil for teaching me how to do PEO on stainless steel and laying the foundation for this thesis, and dealing with my poor Portuguese speaking, Oi tudo bem.

Thank you to my committee members Dr. Walajabad S. Sampath and Dr. Yan (Vivian) Li for serving as my committee members. Thank you to Dr. Rebecca Miller for teaching me how to use the XPS and SEM and answering my persistent questions Dr. Brian Newell for teaching me how to use XRD.

To my lab mates and my other colleagues in the Scott building. Dr. Roberta Sabino & Dr. Liszt Madruga thank you for the help with doing my cell studies. Vignesh Manivasagam and Aniruddha Savargaonkar thank you for the help with my bacterial studies. Thank you to Justyn Knapp for helping with fabrication of my samples. Thanks to my colleagues Harvinder Virk and Abhishek Bhattacharjee, for all the support.

DEDICATION

I am dedicating this thesis to my grandfather Dr. Stephen P Berardinelli and my fiancée Dr. Veronica Martin who have been my main supporters throughout my academic journey.

TABLE OF CONTENTS

ABSTRACT.....	ii
ACKNOWLEDGEMENTS.....	iii
DEDICATION.....	v
LIST OF TABLES.....	vii
LIST OF FIGURES.....	viii
INTRODUCTION	1
HYPOTHESIS AND SPECIFIC AIMS.....	4
CHAPTER 1.....	6
LITERATURE REVIEW.....	6
1.1 Introduction.....	6
1.2 Orthopedic implant failure.....	7
1.3 Osteointegration of orthopedic implants.....	9
1.4 Bacterial infection on orthopedic implants.....	11
1.5 Metal based biomaterials.....	13
1.6 Surface modification of orthopedic implants.....	15
1.7 Plasma electrolytic oxidation on metal surfaces.....	18
REFERENCES	22
CHAPTER 2.....	32
FABRICATION AND CHARACTERIZATION OF PLASMA ELECTROLYTIC OXIDIZED 316L STAINLESS STEEL.....	32
2.1 Introduction.....	32
2.2 Methods and Materials.....	32
2.3 Results and Discussion.....	35
2.4 Conclusions.....	46
REFERNECES.....	47
CHAPTER 3.....	49

CELLULAR VIABILITY AND DIFFERENATION ON PLASMA ELECTROLYTIC OXIDATION STAINLESS.....	49
3.1 Introduction.....	49
3.2 Methods and Materials.....	44
3.3 Results and Discussion.....	49
3.4 Conclusion.....	68
REFERENCES.....	69
CHAPTER 4.....	71
BACTERIAL ADHESION AND PROLIFERATION ON PLASMA ELECTROLYTIC OXIDATION STAINLESS.....	71
4.1 Introduction.....	71
4.2 Methods and Materials.....	72
4.3 Results and Discussion.....	74
4.4 Conclusion.....	80
REFERENCES.....	81
CHAPTER 5.....	83
CONCLUSIONS AND FUTURE WORK.....	83
5.1 Conclusions.....	83
5.2 Future Work.....	84

LIST OF TABLES

Table 1: XPS elemental composition calculated from survey scans of different surfaces.40

LIST OF FIGURES

- Figure 1.2.1 Graphical representation of various causes of dental implant failure ranging from mechanical failure of the device to immune system rejection. From Baseri, Milad, et. al. "Immunological Aspects of Dental Implant Rejection", *BioMed Research International* (2020) doi: 10.1155/2020/7279509.....9
- Figure 1.3.1 Wang, Yulan & Zhang, Yufeng & Miron, Richard, Health, Maintenance, and Recovery of Soft Tissues around Implants: Soft Tissues around Implants, *Clinical implant dentistry and related research*, (2016), 18(3):618-34. doi: 10.1111/cid.12343.....11
- Figure 1.4.1 Map representation of deaths attributable to antibiotic resistance pathogens. From Tripathy, A., Sen, P., Su, B., & Briscoe, W. H., *Natural and bioinspired nanostructured bactericidal surfaces*, *Advances in colloid and interface science*, (2017), 248, 85-104, <https://doi.org/10.1016/j.cis.2017.07.030>.....13
- Figure 1.6.1 Graphical representation of cell interactions with the different levels of modification that can occur. From Li, J.; Zhou, P.; Attarilar, S.; Shi, H. *Innovative Surface Modification Procedures to Achieve Micro/Nano-Graded Ti-Based Biomedical Alloys and Implants*. *Coatings*, 2021, 11, 647. <https://doi.org/10.3390/coatings110606>.....18
- Figure 1.7.1 Graphical depiction of the plasma electrolytic oxidation process on titanium with a schematic of the DC power setup. From Xiwen Yu et. al., *Formation process of in situ oxide coatings with high porosity using one-step plasma electrolytic oxidation*, *Applied Surface Science*, (2016), <https://doi.org/10.1016/j.apsusc.2016.01.144>.....21

Figure 2.2.1 Schematic of the PEO fabrication process. SS is attached to the anode while graphite is attached to cathode. Both SS and graphite partially submerged in sodium bicarbonate electrolyte solution.....34

Figure 2.3.1 Images SS PEO under constant oxidation and SS PEO pulse timings. The red circle indicates the SS PEO that acquired graphite deposition on the surface.....36

Figure 2.3.2 Images of the PEO 1 second pulse process being conducted with no power and DC power of 120V and 8A.....37

Figure 2.3.3 Images of unmodified 316L SS and PEO SS pulsed at 1 second and 0.5 second time cycles.....38

Figure 2.3.4 SEM images of the different surface at different magnifications (1500x and 5000x). The red circles indicate where the 5000x images were taken.....40

Figure 2.3.5 Contact angles of DI water (10 μ L) droplets on the different surfaces. Significant differences of (***) indicates $p \leq 0.001$) for contact angles. Error bars represent the standard deviation.....42

Figure 2.3.6 XPS survey scans of the different surfaces. Survey spectra was run from 1100eV to 0eV with a pass energy of 187.75eV.....44

Figure 2.3.7 XRD scans of the different ss surfaces. XRD scans were collected in the 2 θ range.....46

Figure 3.3.1 Fluorescence microscopy images, at 10x zoom, adhesion of day 1, 4, and 7 after incubation upon the surfaces. Cytoskeletons appear red, while nuclei appear blue under fluorescence.....55

Figure 3.3.2 Cell counts quantitative comparison. Significant differences of (***) indicates $p \leq 0.001$) for Cell count per cm^2 . Error bars represent the standard deviation.....56

Figure 3.3.3 Cell viability, alamar blue was conducted through a plate reader determining the absorbance of the alamar blue dye at 600 and 570 nm after 6 hours of incubation. Error bars represent the standard deviation.....57

Figure 3.3.4 Representative SEM images of ADSCs on different surfaces at 1500x. The red circles represent were the 5000x images were taken from the 1500x image.....58

Figure 3.3.5 Representative SEM images of ADSCs on different surfaces at 5000x.....59

Figure 3.3.6 Alkaline phosphatase assay quantitative comparison between the different surfaces. Significant differences of (***) indicates $p \leq 0.001$) for ALP content per total protein content. Error bars represent the standard deviation.....61

Figure 3.3.7 Calcium deposition assay quantitative comparison. Significant differences of (***) indicates $p \leq 0.001$) for Calcium concentration per total protein content Error bars represent the standard deviation.....62

Figure 3.3.8 Osteocalcin fluorescence images Fluorescence microscopy images, at 10x zoom, adhesion of week 1 and week 3 after incubation upon the surfaces. Cytoskeletons appear red, nuclei appear blue under fluorescence, while osteocalcin deposits appear green.....63

Figure 3.3.9 Osteocalcin coverage quantitative comparison. Significant differences of (***) indicates $p \leq 0.001$) for osteocalcin area coverage percentages. Error bars represent the standard deviation.....64

Figure 3.3.10 Cell differentiation morphology SEM images 1500x. Red circles indicate where the 5000x images were taken.....66

Figure 3.3.11 Representative SEM images of ADSCs on different surfaces at 5000x.....67

Figure 4.3.1 A) Representative fluorescence images of *S. aureus* on the different surfaces. *S. aureus* adhesion area percentage for live (B) and dead (C) bacteria after 6 and 24 hours. Significant differences of (***) indicates $p \leq 0.001$) for *S. aureus* coverage. Error bars represent the standard deviation.....75

Figure 4.3.2 Figure 4.3.2 Representative SEM images of *S. aureus* on different surfaces at 1500x magnification. The red circles represent where the 5000x images were taken from the 1500x image. (A) Representative SEM images of *S. aureus* on different surfaces at 5,000x magnification (B).....78

INTRODUCTION

Orthopedic implants are widely used medical devices for the treatment of joint trauma, bone fractures, spinal ailments, and dentofacial ailments. These devices can be fabricated from a variety of materials. However, 316L stainless steel has been a consistent material for these devices. Common orthopedic implants that utilize 316L stainless steel are endosseous dental implants, hip implants, etc. [1]. The prominent issue for these devices is implant failure. Orthopedic implant failure has two noticeable causes of failure, lack of osteo integration and bacterial infections [2]. Lack of osteointegration between the host bone tissue and the device will cause lack of bone reabsorption resulting in the bone tissue being unable to fuse with the device [2]. Bacterial infection is when a bacterial species is able to proliferate in spite of the host immune system. The excess growth of bacteria on these devices prevents the host from being able to heal and integrate with the device leading to the implant being rejected [2]. Thus, the development of techniques that enhance osteointegration and prevent bacterial infections for these devices are needed.

Previous studies have shown that surface modifications are viable techniques to enhance osteointegration and prevent bacterial infections [2]. Surface modifications of these devices may include changing the surface morphology, chemistry, and wettability. Surface modifications that have been shown to enhance osteointegration are plasma spraying, anodization, physical vapor deposition, etc. [2]. By these modifications enhancing the osteointegration on the surfaces of materials this may lead to increased bone reabsorption, thus leading to reduced failure rates from lack of osteointegration.

Surface modifications that have been shown to reduce bacterial adhesion include plasma electrolytic oxidation doping with ions, hierarchical nanostructure fabrication, deposition of antimicrobial compounds, etc. [3]. By these modifications reducing the bacterial adhesion on the surfaces of materials this may lead to reduced infection rates of the for these orthopedic implants and potential use of antibiotics to treat these infections.

Plasma electrolytic oxidation is an emerging surface modification methodology, that creates a layer oxidation of on the surface of a material [4]. There is little known how a PEO modified 316L stainless steel surface alone will affect osteointegration or bacterial adhesion. Since 316L stainless steel is a common biomaterial is important to evaluate the osteointegration and the bacterial adhesion to determine if this modification technique will be valid for further development for these devices.

In this study, 316L stainless steel underwent plasma electrolytic oxidation via pulse timings. The modified 316L SS surfaces were characterized using the following techniques: surface wettability via contact angle measurements, surface morphology via SEM, surface chemistry via XPS, and surface crystallinity via XRD. Cell adhesion and viability was characterized using the following techniques: cell adhesion via fluorescence microscopy, cell viability via an alamar blue assay, and cell morphology via SEM. Osteointegration was characterized using the following techniques: cell material deposition was characterized via ALP and calcium assays, cell osteocalcin deposition via fluorescence microscopy, cell morphology via SEM. Bacterial adhesion and morphology were characterized using the following techniques: bacterial adhesion via fluorescence microscopy and bacterial morphology via SEM. The results indicate that PEO modified surfaces of 316L SS were able to maintain the cell adhesion and viability, and

osteointegration, while reducing the adhesion of *S. aureus*. Thus, these modified surfaces have the potential to be utilized for orthopedic implants.

HYPOTHESIS AND SPECIFIC AIMS

Fundamental Hypothesis: Plasma electrolytic oxidized 316l stainless steel can reduce the attachment of bacteria while maintaining adipocyte derived stem cell adhesion, proliferation, and differentiation.

Hypothesis 1: Plasma electrolytic oxidation on 316l stainless steel can be oxidized to create a unique surface topography.

Specific Aim 1: Fabrication and characterization of plasma electrolytic oxidized 316l stainless steel. This specific aim is discussed in Chapter 2 and will cover:

- a. Fabrication of a unique surface topography that is reproducible via plasma electrolytic oxidation
- b. Characterization of plasma electrolytic oxidized stainless steel and measurements of contact angles for water.

Hypothesis 2: Plasma electrolytic oxidized 316l stainless steel maintains ADSC's ability to adhere, proliferate, and differentiate

Specific Aim 2: Characterization of adipocyte derived stem cell adhesion, proliferation, differentiation This specific aim is discussed in chapter 3 and will cover:

- a. Evaluate the initial ADSC viability and proliferation
- b. Determine ADSCs differentiation into osteogenic cells

Hypothesis 3: Plasma electrolytic oxidized 316l stainless steel reduces bacterial adhesion and proliferation.

Specific Aim 3: Characterization of *Staphylococcus aureus* adhesion, proliferation, and morphology. This specific aim is discussed in chapter 4 and will cover:

- a. Adhesion, proliferation, and morphology of *Staphylococcus aureus*

CHAPTER 1

LITERATURE REVIEW

1.1 Introduction

Orthopedic implants are commonplace today for treating individuals with bone traumas and joint ailments. However, the use of orthopedic implants has only been viable in a little over the past century for medicine. The advent of using anesthesia and aseptic surgical techniques in tandem during the late 19th century allowed for more complicated surgeries to occur [4]. The use of orthopedic implants began in the early 20th century when British physician, nurse, and a Belgian surgeon designed a fracture plate of stainless steel to aid in the reconstruction of bone fractures [5]. This design had some flaws with the stainless steel being used, as it was not fully bioinert [5]. Later irritations of implants used different combinations of various metals, such as cobalt and chromium, to improve the biocompatibility of the devices [5].

Later, in the early-mid 20th century the use of screws and nails in tandem with plates was done by Ernest Groves and Marius Smith-Petersen [5]. By 1939 the idea arthroplasty had been established, in that devices would be utilized to replace full joints that had been worn out, to some avail with 30 to 40% of patients regaining full function in those joints [5]. Following the second world war, the mass expense of materials allowed for the

development of more complicated implants beyond the use of nails, screws, and plates, along with the use of antibiotics allowed for more invasive surgeries to occur [5].

The current practices surrounding orthopedic implants have progressed significantly since the origin of these devices. Improvements in sterilization, device design and material choice, as well as surgical techniques have progressed the lifespan of orthopedic implants from being used until the fracture has healed to replacing joints for multiple decades [5]. Orthopedic implants have evolved from using metals alone to a variety of materials being used in tandem with each material serving a specific purpose. For example, total hip arthroplasties have been conducted in the US since 1969, and since then the procedure and devices have progressed from being a fully metal device to now being conducted with a titanium stem and ceramic on ceramic ball and socket [6,7].

Currently, orthopedic implantable devices include a few general categories: devices for healing bone fractures, full joint replacements and arthroplasties, spine replacements and stabilizers, and dentofacial implants [1,8]. Common materials for these devices include metals such as titanium and various metal alloys, stainless steel and chrome-cobalt, polymers such as polyetheretherketone, biodegradable materials including metals, such as magnesium and zinc, polymers, such as Inion CPS® and Synthes Rapidsorb® [9]. However, while these materials are viable there exists downsides to them, for example titanium is an expensive material to be used [10].

1.2 Orthopedic implant failure

Ensuring that orthopedic implants integrate with the human body and serve their purpose is vital. Implant failure is the failure of an implantable device to serve its function after surgery. It is estimated that up to 10% of implants will fail [11]. In the US it was estimated that orthopedic trauma implants sales were \$3.3 billion dollars in 2012, with sales increasing annually since then [11].

With these financial considerations and failure rates the contending challenge is ensuring the success of these devices after surgery. Orthopedic implants can fail due to various causes. Devices can fail mechanical failures of the material used, poor implantation during the surgery or other surgical errors, along with the parts of the device creating particles and shards that spread throughout the surrounding tissue [13,14,15]. Patient immune systems and genetics can lead to the tissue rejecting the device. Some patients have sensitivities and allergies that cause the immune system to have excessive reactions by the innate immune system causing increased inflammation or with the adaptative immune system causing the recruitment of B and T cells to the area causing rejection of the device [16]. Poor patient post after care may lead to these devices failing. By patients not tending wounds, not following post operation instructions, or exposing the wounds to excessive environmental stress, such as smoking, can lead to increased healing times which can prevent osteointegration or allow a bacterial infection to occur [17].

The two of the most prominent causes of failure involve lack of osteointegration of the surrounding tissue and the implantable device and a bacterial infection occurring on these devices [18,19]. These modes of failure will be discussed in their respective

sections as current literature focuses on improving the osteointegration and antimicrobial properties of these devices through a variety of methods.

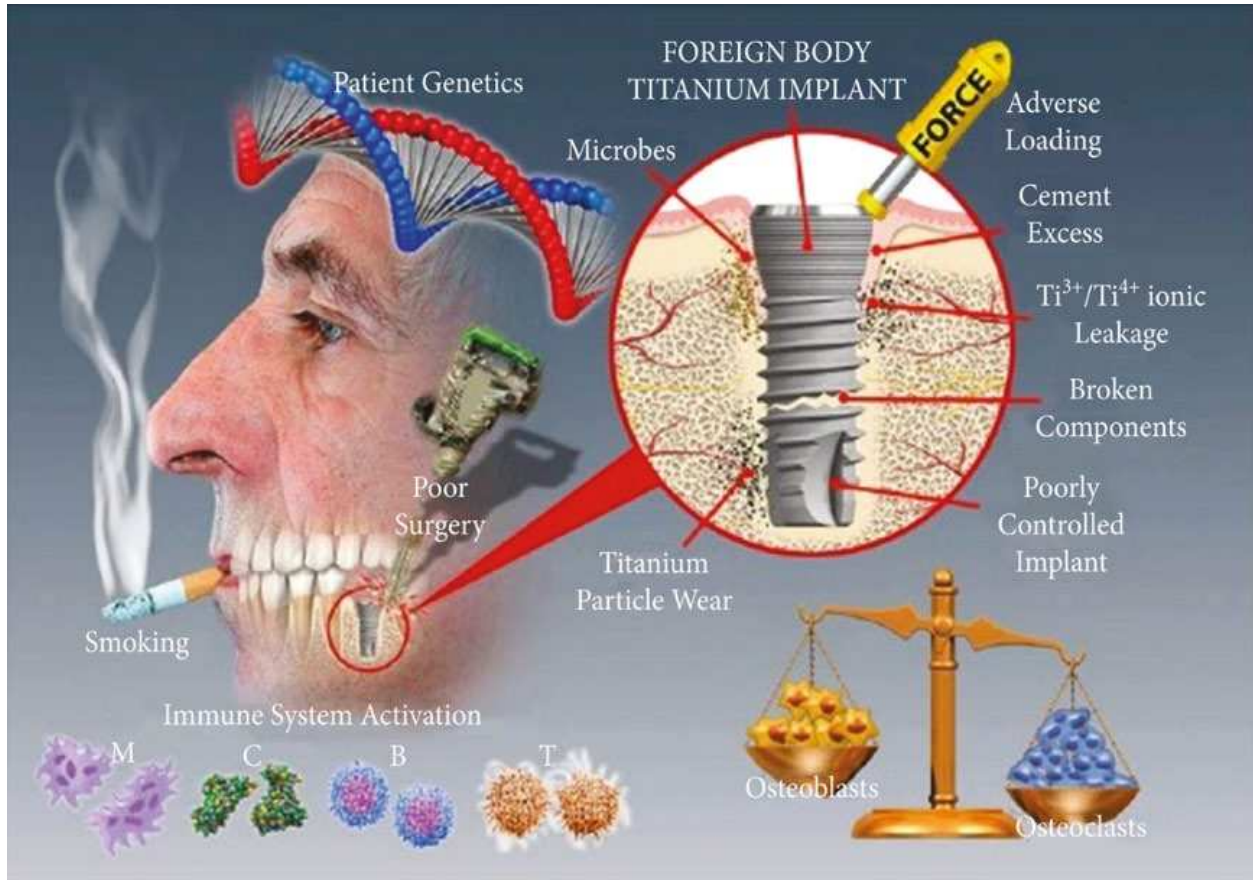


Figure 1.2.1 Graphical representation of various causes of dental implant failure ranging from mechanical failure of the device to immune system rejection. From Baseri, Milad, et. al. Immunological Aspects of Dental Implant Rejection, BioMed Research International (2020) doi: 10.1155/2020/7279509.

1.3 Osteointegration of orthopedic implants

The osteointegration capability of an orthopedic implant is a critical component for ensuring the success of the device. Osteointegration is the acceptance and eventually fusing of the surrounding bone tissue around the implant merging with the implant itself to provide structural stability [20]. Before a device is implanted into the body a section of

the bone tissue is removed to make space for the implementation, then the device is implanted into the bone tissue [21].

The healing phases after an implant is placed within the human body follows a known trend. Initially after the surgery, the body will have the innate immune system react around the implant with macrophages and neutrophils surrounding the tissue; during this phase it is vital that the biomaterial is bioinert as not to cause an overreaction from the immune system that leads to the device being rejected from the body [21]. Afterwards the bone tissue will begin angiogenesis around the device allowing for nutrients and other cell signals to circulate, thus recruiting mesenchymal cells as well as osteoblasts, osteoclasts, and other bone related cells [22]. Osteoblasts will then begin forming new bone tissue from the implant towards the surrounding tissue and vice versa [22].

Current strategies to improve osteointegration include adding in drugs, changes in the surgical techniques/equipment for implantation, surface modifications of the materials used on the implants. Hydroxyapatite is one such compound used to enhance osteointegration of biomaterials as it is bioavailable form of calcium apatite whose role is to provide structural stability for bone tissue [23]. Hydroxyapatite can be deposited onto surface in a variety of methods depending on the material being use, for example metal-based biomaterials for orthopedic implants use a wet chemical deposition of biomimetic to achieve hydroxyapatite that is seen *in vivo* [23]. Other methods of hydroxyapatite coating combine hydroxy apatite to other trace elements such as copper and zinc [24]. Surface modifications have been shown to increase the osteointegration of materials as well, is discussed in more detail in a later section [2]. Recent literature has shown that the combination of surface modifications with the addition of compounds has been shown to

increase osteointegration as seen with tanfloc on titanium nanotubes enhance the osteointegration of differentiated adipocyte derived stem cells *in vitro* [25]. Tanfloc is a cationic polyphenol known to enhance biocompatibility and antimicrobial properties [25].

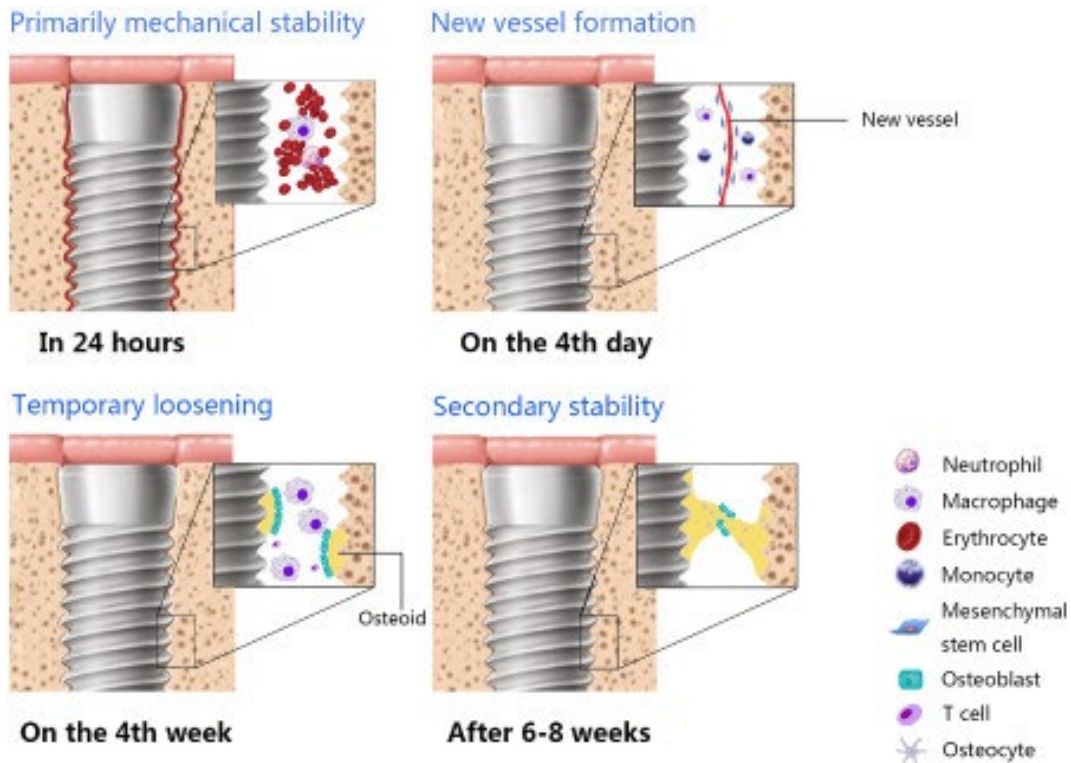


Figure 1.3.1 Graphical representation of the healing phases after dental implant has been surgically implanted. From Wang, Yulan & Zhang, Yufeng & Miron, Richard, Health, Maintenance, and Recovery of Soft Tissues around Implants: Soft Tissues around Implants, Clinical implant dentistry and related research, (2016), 18(3):618-34. doi: 10.1111/cid.12343.

1.4 Bacterial infection on orthopedic implants

Due to the invasive nature of implant procedures, it leaves for a perfect storm for a bacterial infection to occur. Bacterial infections that occur on orthopedic implants can either be nosocomial or due to poor wound care by the patient post operation [3]. Nosocomial infections are commonly called hospital acquired infections [3]. The

challenge with preventing a bacterial nosocomial infection on an orthopedic implant is that it can come from practically anywhere in the hospital environment; ranging from the medical devices themselves to the instruments used by physicians to implant these devices to contaminated clothing or operating rooms [3].

This challenge of a bacterial infection is compounded by the rising prevalence of antibiotic resistance of pathogens, thus increasing the severity of infections that can occur on orthopedic implants [26]. The increasing prevalence of antibiotic infections is a global issue that is predicted to increase deaths every year with yearly fatalities into the several millions for the underdeveloped parts of the world, while more developed parts of the world will suffer fatalities in the hundreds of thousands [26].

Common nosocomial antibiotic resistant pathogens include *Pseudomonas aeruginosa* a gram-negative bacterial species and *Staphylococcus aureus* a gram-positive bacterial species [27,28]. Gram-negative and gram-positive are prominent classes of bacterial species as they relate to the content of peptidoglycan contained within the cell wall/s of a bacterium [27, 28]. Both *Pseudomonas aeruginosa* and *Staphylococcus aureus* are notable for their biofilm formation on surfaces, *Pseudomonas aeruginosa* is commonly seen forming biofilms within the lungs of individuals who are placed on ventilators while in hospice [27].

The prominent mode of action for antibiotics is to act on the peptidoglycan within the cell walls of a bacterium thus leaving the bacterium unstable leading to eventual death of the bacterium [29]. *Staphylococcus aureus* is a species with prominent antibiotic resistant strains of methicillin-resistant *Staphylococcus aureus* (MRSA) and vancomycin-resistant *Staphylococcus aureus* (VRSA), with methicillin and vancomycin being potent

antibiotics [30]. Thus, leading to the need for novel methods to prevent antibiotic resistant bacterial infections.

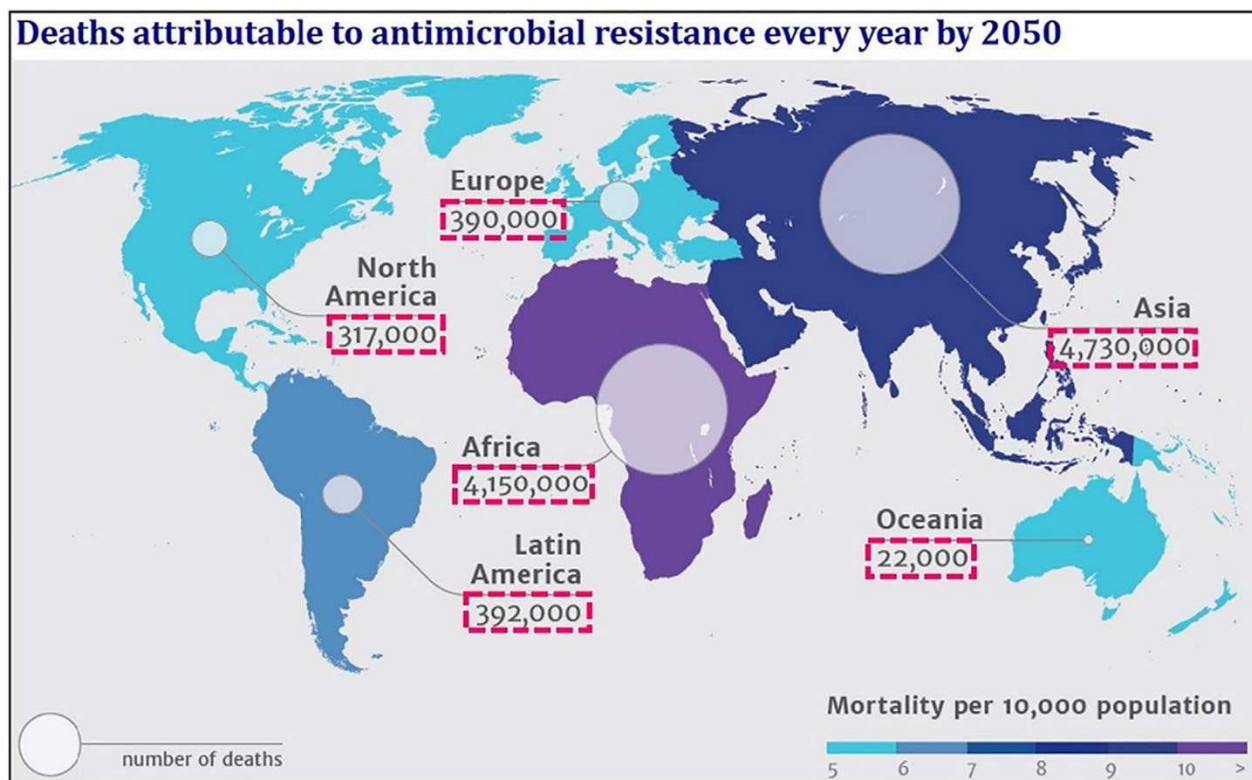


Figure 1.4.1 Map representation of deaths attributable to antibiotic resistance pathogens. From Tripathy, A., Sen, P., Su, B., & Briscoe, W. H., Natural and bioinspired nanostructured bactericidal surfaces, *Advances in colloid and interface science*, (2017), 248, 85-104, <https://doi.org/10.1016/j.cis.2017.07.030>

1.5 Metal based biomaterials

Metal based biomaterials have been used since the beginning of the orthopedic implants. This was to provide structural support for the tissues that are critical to providing structural support for the human body [5]. As previously stated, stainless steel was the original biomaterial used in first plate design back in the late 19th century, however as the

field progressed the use of other metals became common. As of today, implantable devices use a variety of metals in various combinations to serve specific roles, as certain metals such as magnesium, titanium, stainless steel, cobalt chrome, tantalum, etc [31, 32].

Two of the most common metal-based biomaterials used today for these devices are titanium and 316l stainless steel [1]. These metals have similar properties of being bioinert, being resistant to corrosion, and high structural stability [33]. Titanium is the most common biomaterial to be utilized in more developed regions of the world [33]. However, due to the cost of the material it becomes less available for those in underdeveloped regions of the world who may need implantable devices, hence the use of cost-effective metals are more common in these regions [21].

316L stainless steel is a marine grade steel, that is used in surgical equipment and implantable devices [34]. An estimated 60% of devices use 316L stainless steel as the base material [35]. The elemental composition of 316L stainless steel is primarily iron, followed by chromium and nickel, small amounts of manganese and molybdenum, and trace amounts of silicon, nitrogen, phosphorus, sulfur, and carbon [36]. The L in 316L represents a lower carbon concentration as compared to 316 stainless steel [36]. This difference in carbon concentration makes the alloy more resistant to sensitization, which is corrosion of the grains on the outer surface [36]. Resistance to corrosion is a desirable property for a biomaterial as it prevents ion leakages which in high enough concentrations may negatively influence the surrounding tissue, along with potentially compromising the structural stability of the device [37]. One of the prominent fields of research to reduce the failure rates of implantable devices is through surface modification of the biomaterial.

1.6 Surface modification of orthopedic implants

Surface modification is a wide field that may involve changing the surface morphology, chemistry, wettability, the addition of chemicals or drug products, and any combination of what has been listed [38]. The goal of these modifications is to enhance the biocompatibility or the antibacterial properties of the material. These modifications may be targeted towards a specific scale or multiple scales of the surface material; these scales include the microscale seen in micrometers, the sub microscale seen below a micrometer but greater than a nanometer, and the nanoscale seen in nanometers [23]. Each scale is targeted towards different aspects of the surrounding tissue that will interact with the surface. The nano scale of the surface affects how cell materials, such as proteins will bind to the surface; for example, a hydrophobic surface bind more tightly to these materials than a hydrophilic surface, making the materials virtually impossible to remove [39]. The sub microscale of the surface affects how individual cells will adhere and proliferate onto the surface, for example larger cells such as osteoblasts have been seen have improved osteointegration [39]. The micro scale of surface affects the overall components of bone tissue as whole will interact in terms of building new tissue, for example rougher surfaces have seen increases in bone fixation upon the surfaces [39].

Surface modifications can be utilized to improve the osteointegration of orthopedic implants, this improvement will in turn lead to improvements of the success rates of these implants. Surface modifications can be utilized to improve the biocompatibility of orthopedic implants by mimicking the structures seen *in vivo* for bone tissue [36]. This mimicking of the surfaces allows for mesenchymal stem cells and osteoblasts to sense

that they are on bone tissue thus stimulating differentiation and the formation of new bone tissue [40].

Surface modifications have been well explored on the metal-based biomaterials of titanium and stainless steel, as these metals are two of the most common metals to be used in biomaterials [3]. Surface modifications that have been shown to increase osteointegration for titanium include titania nanotube fabrication, acid etching and sand blasting, three-dimensional printing, laser surface texturing, and plasma spraying [39,41,42,43]. Surface modifications that have been utilized on stainless steel include severe shot peening and electrochemical grain boundary etching to create a rougher surface, plasma immersion ion implantation and plasma assisted chemical vapor deposition have been used to create a more corrosion resistant surface [44].

Outside of titanium and stainless steel, surface modifications of acid etching, fluoride and alkaline treatments, as well as laser surface processing have been utilized on magnesium alloys [45]. Polyetheretherketone is another common material used in orthopedic implants that has surface modifications of surface coatings of hydroxy apatite, silicate, and titanium, sulfonation modifications, acid treatments, and nanostructure fabrications [46].

Commercially available surface modifications of titanium include the NanoMetalene® by SeaSpine Holdings using atomic fusion deposition to deposit a layer of pure titanium on the surface of their device changing the morphology of their polyetheretherketone spine implant to make the surface hydrophilic from the original hydrophobic state [47]. Other commercial methods include physical vapor deposition of

titanium-niobium on cobalt-chrome alloys and additive manufacturing allows for open cell porous structures to be fabricated as an implant is being manufactured [48].

Surface modifications can be utilized to enhance the antibacterial properties of a material as well. The goal of these modifications is to prevent bacteria from adhering, this can be achieved by fabricating a surface that has differences in wettability or through the deposition of particles onto the surface [26, 42]. Bioinspired surfaces have been used as an inspiration for surface modification; the surface topographies found on cicada and dragon fly wings have given rise to nanopillar fabrications [Tripathy]. These nanopillars and their relatives of nanowires, nanopores, and nanoglass focus on making a surface that is lethal towards bacteria by creating a surface that is so hydrophilic or hydrophobic that bacterial cells will rupture due to the differences in wettability [26]. These nanopillar based surface modifications are fabricated dependent on the base material, for example titania nanowire arrays are fabricated using a hydrothermal process, whereas a nanopore structured polymer are fabricated using nanoimprint lithography, and nanoglass use reactive ion etching [26]. Another route to enhance the antimicrobial properties of a surface is through depositing particles onto the surface to be released. The addition of metal particles such as silver or copper and their respective oxides have been utilized to prevent biofilm formation, by the ions being released from the surface and binding to the cell membranes of bacteria leading to their eventual death [49].

A known surface modification technique that has been used to enhance both osteointegration and antimicrobial properties of metal-based surfaces is plasma electrolytic oxidation (PEO). PEO has been studied on titanium extensively for applications in biomaterials, while stainless steel has been less studied in comparison [4].

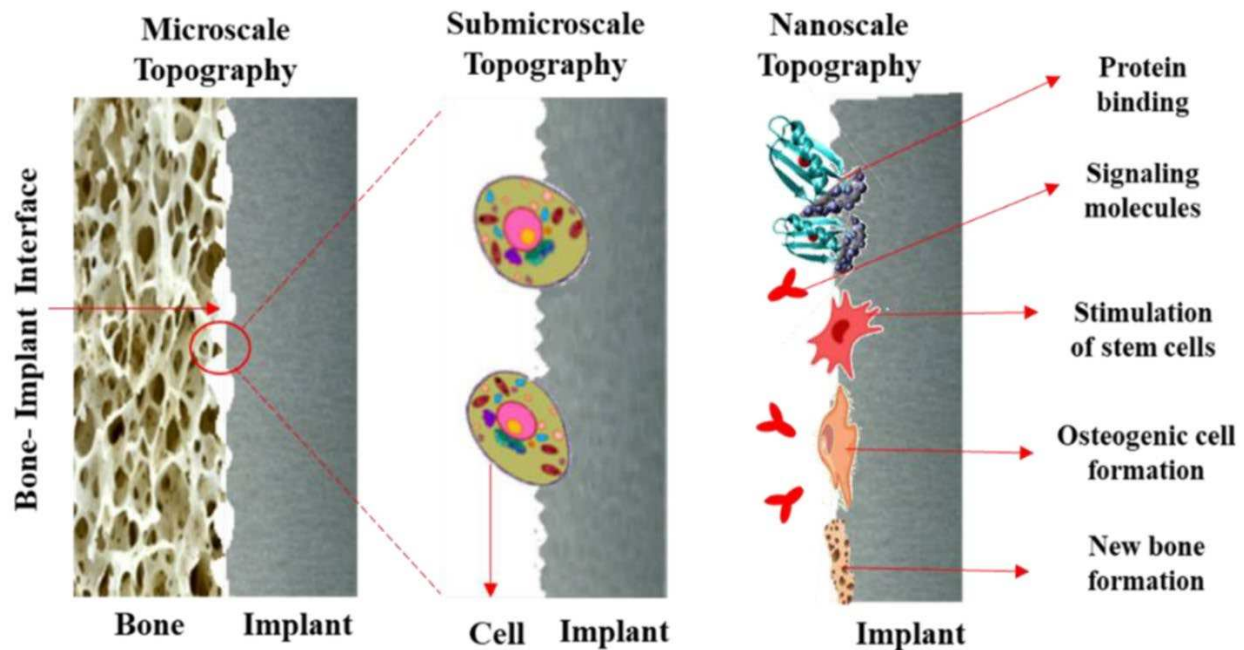


Figure 1.6.1 Graphical representation of cell interactions with the different levels of modification that can occur. From Li, J.; Zhou, P.; Attarilar, S.; Shi, H. Innovative Surface Modification Procedures to Achieve Micro/Nano-Graded Ti-Based Biomedical Alloys and Implants. *Coatings* (2021), 11, 647. <https://doi.org/10.3390/coatings110606>

1.7 Plasma electrolytic oxidation on metal surfaces

A common methodology for modifying metal surfaces is plasma electrolytic oxidation (PEO). The benefits of using PEO as a surface modification include its cost effectiveness, time to manufacture, and ability to add other ions or coatings to the surface [50]. The time to manufacture a single sample from PEO can range in the minutes making the feasibility of mass production attainable. Some surface modifications such as titanium nanotubes can take up to a day to make a single sample [51]. PEO works by oxidizing the outer layer of the metal via a direct current in an electrolyte solution as a conductor

[4]. The current used is of a high enough power that a plasma is formed on the outer layer which penetrates the outer creating a layer of oxidized material, while also removing parts of the surface as well [4]. This fabricated surface creates a layer that is more resistant to corrosion and wear [52]. The materials needed to run PEO procedure include a DC power supply, an electrolyte solution, the desired material to modify, and a counter electrode [4]. The setup for PEO can vary depending on the metal used and the desired effect, for example some PEO setups use cycling electrolyte solution to keep consistent temperatures where others do not, as well as the arrangement of the electrode and counter can vary [53]. PEO has been an area of research since the 1930s; in the late 1990s, PEO research began to focus on creating ceramic like coatings for various metals and their alloys such as aluminum and titanium [54]. Since then, PEO research has progressed extensively and has been used on other metals and alloys such as magnesium, brass, and stainless steel [53]. PEO recently has been using a method to fabricate unique coating for biomaterials, specifically titanium [53].

PEO research for titanium coating for biomaterials has been extensive. The electrolyte solution can be used as a source to deposit ions that may enhance the osteointegration of the surface or add additional antimicrobial properties to the surface [54,55]. As well as titanium oxide being used as a coating for other metals, as seen with a titanium oxide layer that was deposited onto the surface of 316L stainless steel stents [56]. Particles that have been shown to enhance osteointegration of titanium and its alloys include hydroxy apatite, calcium phosphates, magnesium, and silicon [57,58]. Hydroxy apatite is a prominent bone protein produced by osteoblasts; calcium phosphates are main constituents of hydroxy apatite [53]. Magnesium is present throughout bone tissue

and can act as a replacement for calcium in hydroxy apatite [57]. Silicon is known to be present in the metabolic processes of osteoblasts as well [59]. Particles that have been shown to enhance the antibacterial activity of titanium and its alloys include silver, silver oxide, copper, copper oxide, and zinc oxide [60]. These particles act on the membranes of bacteria, leading to the eventually death of the bacteria [60]. These PEO modifications on titanium demonstrate that beyond modifying surface the addition of materials can be used to enhance osteointegration and antibacterial properties.

Of interest is PEO modification on 316L stainless steel to be utilized as a biomaterial for orthopedic implants; it has been shown that PEO on 316L stainless steel has been conducted successfully. As mentioned previously 316L stainless steel has undergone PEO to gain a coating layer of titanium oxide to enhance its biocompatibility for stent applications [47]. However, there is a gap in the literature for how a PEO modified 316L stainless steel will work as a biomaterial. With the prevalence of 316L stainless steel as a base for biomaterial, this knowledge may be fruitful in addressing the issue of orthopedic failure due to osteointegration and bacterial infection.

The focus of this study is to understand how the PEO modified 316L stainless steel surface alone will affect osteointegration and bacterial adhesion. This is due to the prevalence of coatings used in PEO methodology; hence it is of interest as to how the surface alone affects these properties alone as this knowledge will aid later PEO research on the addition of coatings of ion depositions onto the 316L stainless steel surface.

The first aim of this study is to develop a PEO modified surface that maintains its surface chemistry and surface crystallinity when compared to 316L stainless steel. The second and third aims of this study are to determine the effects of PEO modified 316L

stainless on osteointegration as well the bacterial adhesion, respectively. From this knowledge it can be ascertained how the changes of the surface morphology alone may affect osteointegration and bacterial adhesion as the deposition of materials onto surfaces via PEO is a common methodology seen in literature. Hence, this knowledge will aid in the understanding of how the PEO modification can be utilized for 316L based orthopedic implants.

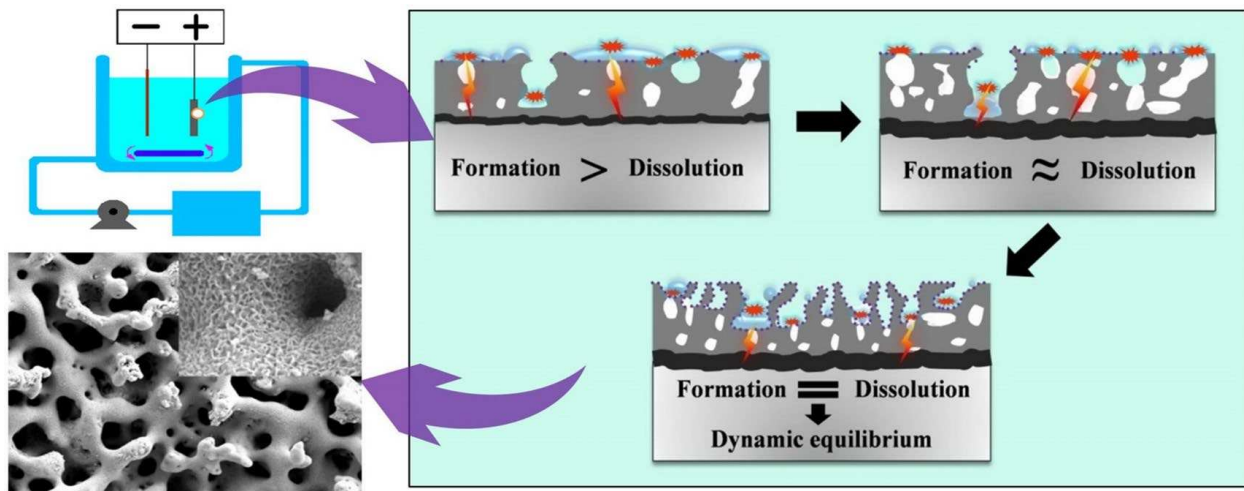


Figure 1.7.1 Graphical depiction of the plasma electrolytic oxidation process on titanium with a schematic of the DC power setup. From Xiwen Yu et. al., Formation process of in situ oxide coatings with high porosity using one-step plasma electrolytic oxidation, Applied Surface Science, (2016), <https://doi.org/10.1016/j.apsusc.2016.01.144>

REFERENCES

- [1] N.S. Manam, W.S.W. Harun, D.N.A. Shri, S.A.C. Ghani, T. Kurniawan, M.H. Ismail, M.H.I. Ibrahim, Study of corrosion in biocompatible metals for implants: A review, *Journal of Alloys and Compounds*, (2017), 701, 698-715, <https://doi.org/10.1016/j.jallcom.2017.01.196>.
- [2] James Quinn, Ryan McFadden, Chi-Wai Chan, Louise Carson, Titanium for Orthopedic Applications: An Overview of Surface Modification to Improve Biocompatibility and Prevent Bacterial Biofilm Formation, *iScience*, (2020), 23, 11, 101745, <https://doi.org/10.1016/j.isci.2020.101745>
- [3] C. Adlhart, J. Verran, N.F. Azevedo, H. Olmez, M.M. Keinänen-Toivola, I. Gouveia, L.F. Melo, F. Crijns, Surface modifications for antimicrobial effects in the healthcare setting: a critical overview, *Journal of Hospital Infection*, (2018), 99, 3, 239-249, <https://doi.org/10.1016/j.jhin.2018.01.018>.
- [4] Xiwen Yu, Li Chen, Honglei Qin, Mingyue Wu, Zongcheng Yan, Formation process of in situ oxide coatings with high porosity using one-step plasma electrolytic oxidation, *Applied Surface Science*, (2016), 366, 432-438, <https://doi.org/10.1016/j.apsusc.2016.01.144>
- [5] Markatos K, Tsoucalas G, Sgantzios M., Hallmarks in the history of orthopaedic implants for trauma and joint replacement. *Acta Med Hist Adriat*, (2016), 14, 1, 161-76
- [6] Siopack JS, Jergesen HE. Total hip arthroplasty. *West J Med.*, (1995), 162, 3, 243

[7] Gwam CU, Mistry JB, Mohamed NS, Thomas M, Bigart KC, Mont MA, Delanois RE, Current Epidemiology of Revision Total Hip Arthroplasty in the United States: National Inpatient Sample 2009 to 2013, *The Journal of Arthroplasty*, (2017), 32, 7, 2088-2092, <https://doi.org/10.1016/j.arth.2017.02.046>.

[8] Peto, Marinela & Ramirez-Cedillo, Erick & Hernández, Adriana & Siller, Hector, Structural design optimization of knee replacement implants for Additive Manufacturing, *Procedia Manufacturing*, (2019), 34, 574-583. <https://doi.org/10.1016/j.promfg.2019.06.222>

[9] Tiffany Kim, Carmine Wang See, Xiaochun Li, Donghui Zhu, Orthopedic implants and devices for bone fractures and defects: Past, present, and perspective, *Engineered Regeneration*, (2020), 1, 6-18, <https://doi.org/10.1016/j.engreg.2020.05.003>.

[10] Chuan Yin, Teng Zhang, Qingguang Wei, Hong Cai, Yan Cheng, Yun Tian, Huijie Leng, Caimei Wang, Shiqing Feng, Zhongjun Liu, Surface treatment of 3D printed porous Ti6Al4V implants by ultraviolet photofunctionalization for improved osseointegration, *Bioactive Materials*, (2022), 7, 26-38, <https://doi.org/10.1016/j.bioactmat.2021.05.043>.

[11] Sakka S, Baroudi K, Nassani MZ. Factors associated with early and late failure of dental implants., *J Investig Clin Dent.*, (2012), 3(4), 258-61, doi: 10.1111/j.2041-1626.2012.00162.

[12] Mark Ayoub, William Paul Bassett, Patricia Seuffert, Douglas Matijakovich, Dorene A. O'Hara, Mark S. Butler, Perception Versus Reality in the Cost of Orthopedic Trauma Implants, *Journal of Surgical Education*, (2018), 75, 5,1333-1341, <https://doi.org/10.1016/j.jsurg.2018.02.015>.

- [13] Sailer, I, Karasan, D, Todorovic, A, Ligoutsikou, M, Pjetursson, BE. Prosthetic failures in dental implant therapy, *Periodontol 2000*, (2022), 88, 130–144, doi:10.1111/prd.12416
- [14] Alison J Smith, Paul Dieppe, Kelly Vernon, Martyn Porter, Ashley W Blom, Failure rates of stemmed metal-on-metal hip replacements: analysis of data from the National Joint Registry of England and Wales, *The Lancet*, (2012), 379, 9822, 1199-1204, [https://doi.org/10.1016/S0140-6736\(12\)60353-5](https://doi.org/10.1016/S0140-6736(12)60353-5).
- [15] Kaymaz I, Bayrak O, Karsan O, Celik A, Alsaran A., Failure analysis of the cement mantle in total hip arthroplasty with an efficient probabilistic method, *Proceedings of the Institution of Mechanical Engineers, Part H: Journal of Engineering in Medicine*, (2014), 228, 4, 409-417, doi:10.1177/0954411914529428
- [16] Baseri M, Radmand F, Hamed R, Yousefi M, Kafil HS. Immunological Aspects of Dental Implant Rejection, *Biomed Res Int.*, (2020), 9, 7279509, doi:10.1155/2020/7279509.
- [17] Tinsley, D., Watson, C.J. and Ogden, A.R., A survey of U.K. centres on implant failures. *Journal of Oral Rehabilitation*, (1999), 26: 14-18. <https://doi.org/10.1046/j.1365-2842.1999.00355.x>
- [18] Chrcanovic, B.R., Albrektsson, T. and Wennerberg, A., Reasons for failures of oral implants. *J Oral Rehabil*, (2014), 41, 443-476, <https://doi.org/10.1111/joor.12157>
- [19] Schwartz-Arad, Devorah DMD, PhD*; Laviv, Amir DMD†; Levin, Liran DMD‡, Failure Causes, Timing, and Cluster Behavior: An 8-Year Study of Dental Implants, *Implant Dentistry*, (2008), 17, 2, 200-207, doi: 10.1097/ID.0b013e3181777906

[20] Wenhao Wang, Kelvin W.K. Yeung, Bone grafts and biomaterials substitutes for bone defect repair: A review, *Bioactive Materials*, (2017), 2, 4, 224-247, <https://doi.org/10.1016/j.bioactmat.2017.05.007>.

[21] Chuan Yin, Teng Zhang, Qingguang Wei, Hong Cai, Yan Cheng, Yun Tian, Huijie Leng, Caimei Wang, Shiqing Feng, Zhongjun Liu, Surface treatment of 3D printed porous Ti6Al4V implants by ultraviolet photofunctionalization for improved osseointegration, *Bioactive Materials*, (2022), 7, 26-38, <https://doi.org/10.1016/j.bioactmat.2021.05.043>

[22] Jia Xu, et. al., Advances of adipose-derived mesenchymal stem cells-based biomaterial scaffolds for oral and maxillofacial tissue engineering, *Bioactive Materials*, (2021), 6, 8, <https://doi.org/10.1016/j.bioactmat.2021.01.015>

[23] Zhang BG, Myers DE, Wallace GG, Brandt M, Choong PF., Bioactive coatings for orthopaedic implants-recent trends in development of implant coatings, *Int J Mol Sci*, (2014), 4, 15(7), 11878-921, doi: 10.3390/ijms150711878.

[24] Daniel Arcos and María Vallet-Regí, Substituted hydroxyapatite coatings of bone implants, *J. Mater. Chem. B*, (2020), 8, 1781-1800, <https://doi.org/10.1039/C9TB02710F>

[25] Roberta M. Sabino, Gabriela Mondini, Matt J. Kipper, Alessandro F. Martins, Ketul C. Popat, Tanfloc/heparin polyelectrolyte multilayers improve osteogenic differentiation of adipose-derived stem cells on titania nanotube surfaces, *Carbohydrate Polymers*, (2021), 251, 117079, <https://doi.org/10.1016/j.carbpol.2020.117079>.

[26] Tripathy, A., Sen, P., Su, B., & Briscoe, W. H., Natural and bioinspired nanostructured bactericidal surfaces. *Advances in colloid and interface science*, (2017), 248, 85-104. <https://doi.org/10.1016/j.cis.2017.07.030>

- [27] Zheng Pang, Renee Raudonis, Bernard R. Glick, Tong-Jun Lin, Zhenyu Cheng, Antibiotic resistance in *Pseudomonas aeruginosa*: mechanisms and alternative therapeutic strategies, *Biotechnology Advances*, (2019), 37, 1, 177-192, <https://doi.org/10.1016/j.biotechadv.2018.11.013>.
- [28] Tong SY, Davis JS, Eichenberger E, Holland TL, Fowler VG Jr., *Staphylococcus aureus* infections: epidemiology, pathophysiology, clinical manifestations, and management. *Clin Microbiol Rev.* (2015) , 28(3), 603-61, doi: 10.1128/CMR.00134-14.
- [29] Blair, J., Webber, M., Baylay, A. et al, Molecular mechanisms of antibiotic resistance, *Nat Rev Microbiol*, (2105) 13, 42–51, <https://doi-org.ezproxy2.library.colostate.edu/10.1038/nrmicro3380>
- [30] Santi M. Mandal, Ananta K. Ghosh, Bikas R. Pati, Dissemination of antibiotic resistance in methicillin-resistant *Staphylococcus aureus* and vancomycin-resistant *S aureus* strains isolated from hospital effluents, *American Journal of Infection Control*, (2015), 43, 12,e87-e88, <https://doi.org/10.1016/j.ajic.2015.08.015>.
- [31] R Radha, D Sreekanth, Insight of magnesium alloys and composites for orthopedic implant applications – a review, *Journal of Magnesium and Alloys*, (2017), 5, 3, 286-312, <https://doi.org/10.1016/j.jma.2017.08.003>
- [32] Tapscott DC, Wottowa C. Orthopedic Implant Materials. [Updated 2022 Jul 25]. In: StatPearls [Internet]. Treasure Island (FL): StatPearls Publishing; 2022 Jan-. Available from: <https://www.ncbi.nlm.nih.gov/books/NBK560505/>

- [33] Merola M, Affatato S. Materials for Hip Prostheses: A Review of Wear and Loading Considerations. *Materials (Basel)*. 2019 Feb 5;12(3):495. doi: 10.3390/ma12030495. PMID: 30764574; PMCID: PMC6384837.
- [34] M.J.K. Lodhi, K.M. Deen, M.C. Greenlee-Wacker, Waseem Haider, Additively manufactured 316L stainless steel with improved corrosion resistance and biological response for biomedical applications, *Additive Manufacturing*, (2019), 27, 8-19, <https://doi.org/10.1016/j.addma.2019.02.005>.
- [35] Beaupré G.S., Csongradi J.J. Refracture risk after plate removal in the forearm. *J. Orthop. Trauma.*, (1996), 10, 87–92, doi: 10.1097/00005131-199602000-00003
- [36] Matmatch GmbH, “Difference between AISI 316, AISI 316L and AISI 316LN Stainless Steel”, accessed 10/8/2022, <https://matmatch.com/learn/material/difference-between-aisi-316-316l-316ln-stainless-steel>
- [37] Weller, J, Vasudevan, P, Kreikemeyer, B, et al. The role of bacterial corrosion on recolonization of titanium implant surfaces: An in vitro study. *Clin Implant Dent Relat Res*. (2022), 1- 12, doi:10.1111/cid.13114
- [38] Resnik, M., Benčina, et. al., Strategies for improving antimicrobial properties of stainless steel. *Materials (Basel, Switzerland)*, (2020), 13(13), 2944, doi: 10.3390/ma13132944
- [39] Li , J.; Zhou, P.; Attarilar, S.; Shi, H. Innovative Surface Modification Procedures to Achieve Micro/Nano-Graded Ti-Based Biomedical Alloys and Implants. *Coatings*, (2021), 11, 647. <https://doi.org/10.3390/coatings110606>

[40] Wang, R., Shi, M., Xu, F. et al. Graphdiyne-modified TiO₂ nanofibers with osteoinductive and enhanced photocatalytic antibacterial activities to prevent implant infection. *Nat Commun*, (2020), 11, 4465, <https://doi.org/10.1038/s41467-020-18267->

[41] Ketul C. Popat, Lara Leoni, Craig A. Grimes, Tejal A. Desai, Influence of engineered titania nanotubular surfaces on bone cells, *Biomaterials*, (2007), 28, 21, 3188-3197, <https://doi.org/10.1016/j.biomaterials.2007.03.020>.

[42] Liu, Y, Rath, B, Tingart, M, Eschweiler, J. Role of implants surface modification in osseointegration: A systematic review. *J Biomed Mater Res*. (2020), 108A, 470– 484. <https://doi-org.ezproxy2.library.colostate.edu/10.1002/jbm.a.36829>

[43] Bai, L.; Gong, C.; Chen, X.; Sun, Y.; Zhang, J.; Cai, L.; Zhu, S.; Xie, S.Q. Additive Manufacturing of Customized Metallic Orthopedic Implants: Materials, Structures, and Surface Modifications, *Metals*, (2019), 9, 1004. <https://doi.org/10.3390/met9091004>

[44] Aliya Bekmurzayeva, Wynter J. Duncanson, Helena S. Azevedo, Damira Kanayeva, Surface modification of stainless steel for biomedical applications: Revisiting a century-old material, *Materials Science and Engineering: C*, (2018), 93, 1073-1089, <https://doi.org/10.1016/j.msec.2018.08.049>.

[45] Wang J, Tang J, Zhang P, Li Y, Wang J, Lai Y, Qin L. Surface modification of magnesium alloys developed for bioabsorbable orthopedic implants: A general review. (*J Biomed Mater Res*, (2012), Part B 2012,100B,1691–1701 <https://doi-org.ezproxy2.library.colostate.edu/10.1002/jbm.b.32707>

[46] Zhi Zheng, Pengjia Liu, Xingmin Zhang, Jingguo xin, Yongjie wang, Xiaosong Zou, Xiaohan Mei, Shuling Zhang, Shaokun Zhang, Strategies to improve bioactive and

antibacterial properties of polyetheretherketone (PEEK) for use as orthopedic implants, (2022), *Materials Today Bio*, Volume 16, 100402, <https://doi.org/10.1016/j.mtbio.2022.100402>.

[47] SeaSpine Holdings, Technologies “NantoMetalene”, accessed 10/10/2022, <https://www.seaspine.com/technologies/nanometalene>

[48] Mark Crawford, On the Surface: Treatments and Coatings for Orthopedics, (2020, May 20th), *Orthopedic Design & Technology* https://www.odtmag.com/issues/2020-05-01/view_features/on-the-surface-treatments-and-coatings-for-orthopedics?utm_source=SilverpopMailing&utm_medium=email&utm_campaign=ODT+-+Surface+Coatings+Special+Edition+%285-21-2020%29+%28Final%29&utm_content=&spMailingID=5411668&spUserID=MjQ5MDQ5MDkxNDUS1&spJobID=1020958998&spReportId=MTAyMDk1ODk5OAS2

[49] Qing Y, Cheng L, Li R, Liu G, Zhang Y, Tang X, Wang J, Liu H, Qin Y. Potential antibacterial mechanism of silver nanoparticles and the optimization of orthopedic implants by advanced modification technologies. *Int J Nanomedicine.*, (2018), 5, 13, 3311-3327, doi: 10.2147/IJN.S165125

[50] Anderson Wagner Alves de Menezes, Ivan Alves de Souza, Thércio Henrique de Carvalho Costa, Tharsia Cristiany de Carvalho Costa, Rômulo Ribeiro Magalhães de Sousa, Rubens Maribondo Nascimento, Michelle de Medeiros Aires, Michelle Cequeira Feitor, Study of the deposition of hydroxyapatite by plasma electrolytic oxidation (PEO) in stainless steel AISI 316LVM samples, *Journal of Materials Research and Technology*, (2022), 18, 1578-1589, <https://doi.org/10.1016/j.jmrt.2022.03.011>.

[51] Wei-Chao Gu, Guo-Hua Lv, Huan Chen, Guang-Liang Chen, Wen-Ran Feng, Si-Ze Yang, PEO protective coatings on inner surface of tubes, *Surface and Coatings Technology*, (2007) 201, 15, 6619-6622, <https://doi.org/10.1016/j.surfcoat.2006.09.056>

[52] Aleksey L. Yerokhin, Viktor V. Lyubimov, Roman V. Ashitkov, Phase formation in ceramic coatings during plasma electrolytic oxidation of aluminium alloys, *Ceramics International*, (1998), 24, 1, 1-6, [https://doi.org/10.1016/S0272-8842\(96\)00067-3](https://doi.org/10.1016/S0272-8842(96)00067-3).

[s 53] Xiaopeng Lu, Marta Mohedano, Carsten Blawert, Endzhe Matykina, Raul Arrabal, Karl Ulrich Kainer, Mikhail L. Zheludkevich, Plasma electrolytic oxidation coatings with particle additions – A review, *Surface and Coatings Technology*, (2016), 307, Part C, 1165-1182, <https://doi.org/10.1016/j.surfcoat.2016.08.055>.

[54] C.B. Wei, X.B. Tian, S.Q. Yang, X.B. Wang, Ricky K.Y. Fu, Paul K. Chu, Anode current effects in plasma electrolytic oxidation, *Surface and Coatings Technology*, (2007), 201, 9–11, 5021-5024, <https://doi.org/10.1016/j.surfcoat.2006.07.103>.

[55] Monica Thukkaram, Pieter Cools, Anton Nikiforov, Petra Rigole, Tom Coenye, Pascal Van Der Voort, Gijs Du Laing, Chris Vercruysse, Heidi Declercq, Rino Morent, Lieven De Wilde, Patrick De Baets, Kim Verbeken, Nathalie De Geyter, Antibacterial activity of a porous silver doped TiO₂ coating on titanium substrates synthesized by plasma electrolytic oxidation, *Applied Surface Science*, (2020), 500, 144235 <https://doi.org/10.1016/j.apsusc.2019.144235>.

[56] Huan, Z.; Fratila-Apachitei, L.E.; Apachitei, I.; Duszczyk, J. Characterization of Porous TiO₂ Surfaces Formed on 316L Stainless Steel by Plasma Electrolytic Oxidation

for Stent Applications, *J. Funct. Biomater.*, (2012), 3, 349-360.
<https://doi.org/10.3390/jfb3020349>

[u 57] Ping Huang, Ke-Wei Xu, Yong Han, Preparation and apatite layer formation of plasma electrolytic oxidation film on titanium for biomedical application, *Materials Letters*, (2005), 59, 2–3, 185-189, <https://doi.org/10.1016/j.matlet.2004.09.045>.

[58] Rokosz, K., Hryniewicz, T., Pietrzak, K. and Malorny, W., SEM and EDS Characterization of Porous Coatings Obtained On Titanium by Plasma Electrolytic Oxidation in Electrolyte Containing Concentrated Phosphoric Acid with Zinc Nitrate, *Advances in Materials Science*, (2017), 17, 2, 41-54. <https://doi.org/10.1515/adms-2017-0010>

[59] Seon-Yeong Park, Han-Cheol Choe, Functional element coatings on Ti-alloys for biomaterials by plasma electrolytic oxidation, *Thin Solid Films*, (2020), 699, 137896, <https://doi.org/10.1016/j.tsf.2020.137896>.

[60] Arash Fattah-alhosseini, Maryam Molaei, Navid Attarzadeh, Kazem Babaei, Faridreza Attarzadeh, On the enhanced antibacterial activity of plasma electrolytic oxidation (PEO) coatings that incorporate particles: A review, *Ceramics International*, (2020), 46, 13, 20587-20607, <https://doi.org/10.1016/j.ceramint.2020.05.206>.

CHAPTER 2

FABRICATION AND CHARACTERIZATION OF PLASMA ELECTROLYTIC OXIDIZED 316L STAINLESS STEEL

2.1 Introduction

The surface morphology of biomaterials may influence various responses when a medical device is implanted into the body [1]. One the key factors that surface morphology can influence is the ability of cells and bacteria to adhere and proliferate [2,3]. Research has shown that plasma electrolytic oxidation (PEO) is a simple method for surface morphology modification for various metallic materials [4]. 316L stainless steel (316L SS), commonly known as marine grade or food grade stainless steel, is a widely used metal alloy for biomaterials [5]. 316L SS is utilized both for surgical tools, and implantable devices such as orthopedic hip implants and endosseous dental implants [6,7,8]. There are several properties of 316L SS make it ideal for these uses, these include resistance to corrosion, passivated, and cost effectiveness [9,10].

2.2 Materials & Methods

2.2.1 Fabrication of Plasma Electrolytic Oxidized 316L Stainless Steel Surfaces

The SS surfaces were modified by PEO [11]. SS sheets with 0.15 cm thickness were cut in to 0.5 cm x 10 cm strips. Prior to modification, the surfaces were cleaned via sonication for 5 mins in each acetone, isopropyl alcohol and deionized (DI) water and air

dried. An electrolyte solution of 7.5% by weight of sodium bicarbonate in DI water was used for the PEO process. The electrolyte solution was heated to 90°C before SS and graphite were partially submerged. The SS was used as the anode and a piece of graphite (4 cm x 1.75 cm x 0.3 cm) was used as the cathode, and both were connected to a programmable direct current (DC) power supply (BK Precision, PVS60085MR) (**Figure 2.2.1**). PEO was performed at 180 V and 8 A for three timings:

- 180 seconds of continuous power.
- 550 seconds with a 1 second pulses of DC power cycling between on and off for an oxidation time of 225 seconds. (SS 1s)
- 390 seconds with a 0.5 second pulses of DC power cycling between on and off for an oxidation time of 195 seconds (SS 0.5s)

After completion of the PEO process, the surfaces were rinsed with DI water, dried, and stored until further use.

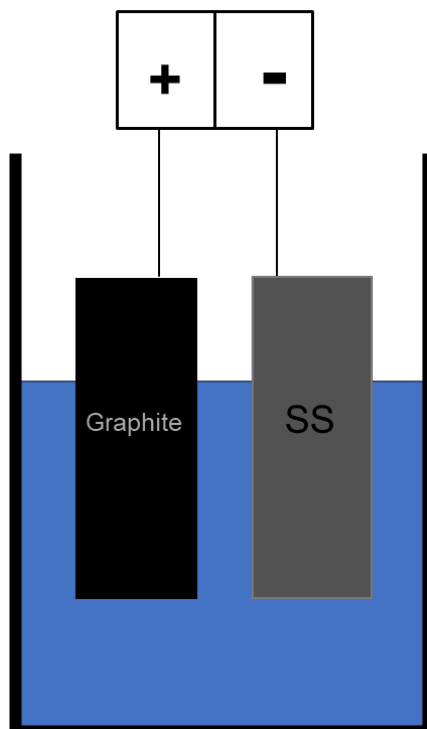


Figure 2.2.1 Schematic of the PEO fabrication process. SS is attached to the anode while graphite is attached to cathode. Both SS and graphite partially submerged in sodium bicarbonate electrolyte solution.

2.2.2 Characterization of Plasma Electrolytic Oxidized 316L Stainless Steel Surfaces

Different surfaces were characterized by their morphology, wettability, surface chemistry, and surface crystallinity.

The surface morphology was characterized using a field emission scanning electron microscope (SEM) (JEOL JSM-6500). Different surfaces were imaged at 15 kV at 1500X and 5000X magnifications. The wettability of different surfaces was characterized using contact angle goniometry (Ramé-Hart Model 250). A 10 μ L drop of DI water was placed on the surface using a micropipette. The image of the water droplet

was taken using the camera attached to the goniometer. The apparent contact angle was measured with the software provided with the goniometer.

The chemical composition of the surfaces was characterized via an X-Ray Photoelectron Spectrometer (PHI Physical Electronics PE-5800 X-ray Photoelectron Spectrometer). Survey scans were collected for different surfaces, ranging from 0 eV to 1100 eV. From the survey scans, the surface composition was determined via CASA XPS software from peak fits.

The crystallinity of different surfaces was characterized using X-ray diffraction (XRD) (Shimadzu XRD7000). XRD scans used a Thin-Film geometry with a 5° incidence angle, with CuK α radiation, with a range of X-Ray angles of 20 to 80° and continuous scanning with speed of 2°/min.

2.2.3 Statistical Analysis

Contact angle measurements were taken on at least three different surfaces, with droplets on at least three different locations on each surface. Tukey tests were conducted for quantitative comparison. An alpha value 0.05 was used and p-values ≤ 0.05 were considered statistically significant. R software was used to conduct all analysis.

2.3 Results and Discussion

2.3.1 Fabrication of Plasma Electrolytic Oxidized 316L Stainless Steel Surfaces

The initial use of a continuous DC power for 180 seconds created undesirable surfaces. The surfaces were covered with large amounts of graphite build up, that was not desired as it would influence differences in the surfaces in further biological studies (**Figure 2.3.1**). Thus, this led to the use of pulse timings for PEO.

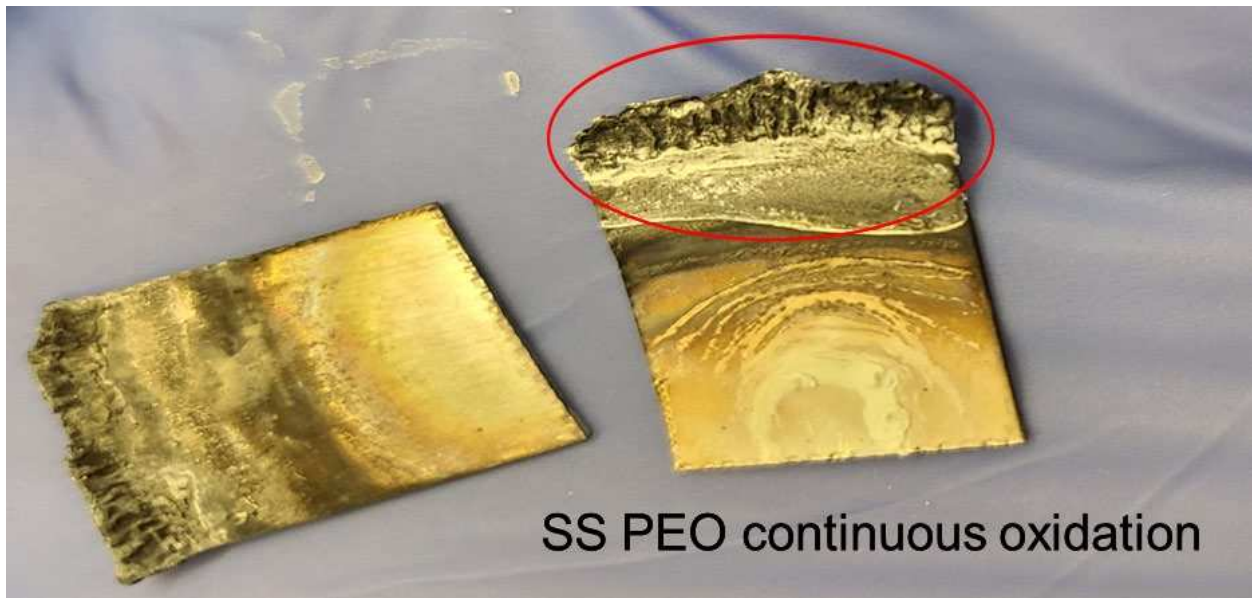


Figure 2.3.1 Images SS PEO under constant oxidation and SS PEO pulse timings. The red circle indicates the SS PEO that acquired graphite deposition on the surface

The power supply used was able to utilize customizable programs where stepwise power can be used to oxidize surfaces for different time periods. A time cycle of 1 second with DC power on and off was used to fabricate the SS 1s surface and a time cycle of 0.5 seconds with DC power on and off was used to fabricate the SS 0.5s surface. As seen in **Figure 2.3.2**, the left image shows when the power is off, and the right image shows when the power is on for the PEO 1 second process. When the power is on, the surface shows sparking indicating the generation of plasma and oxidation of the surface.

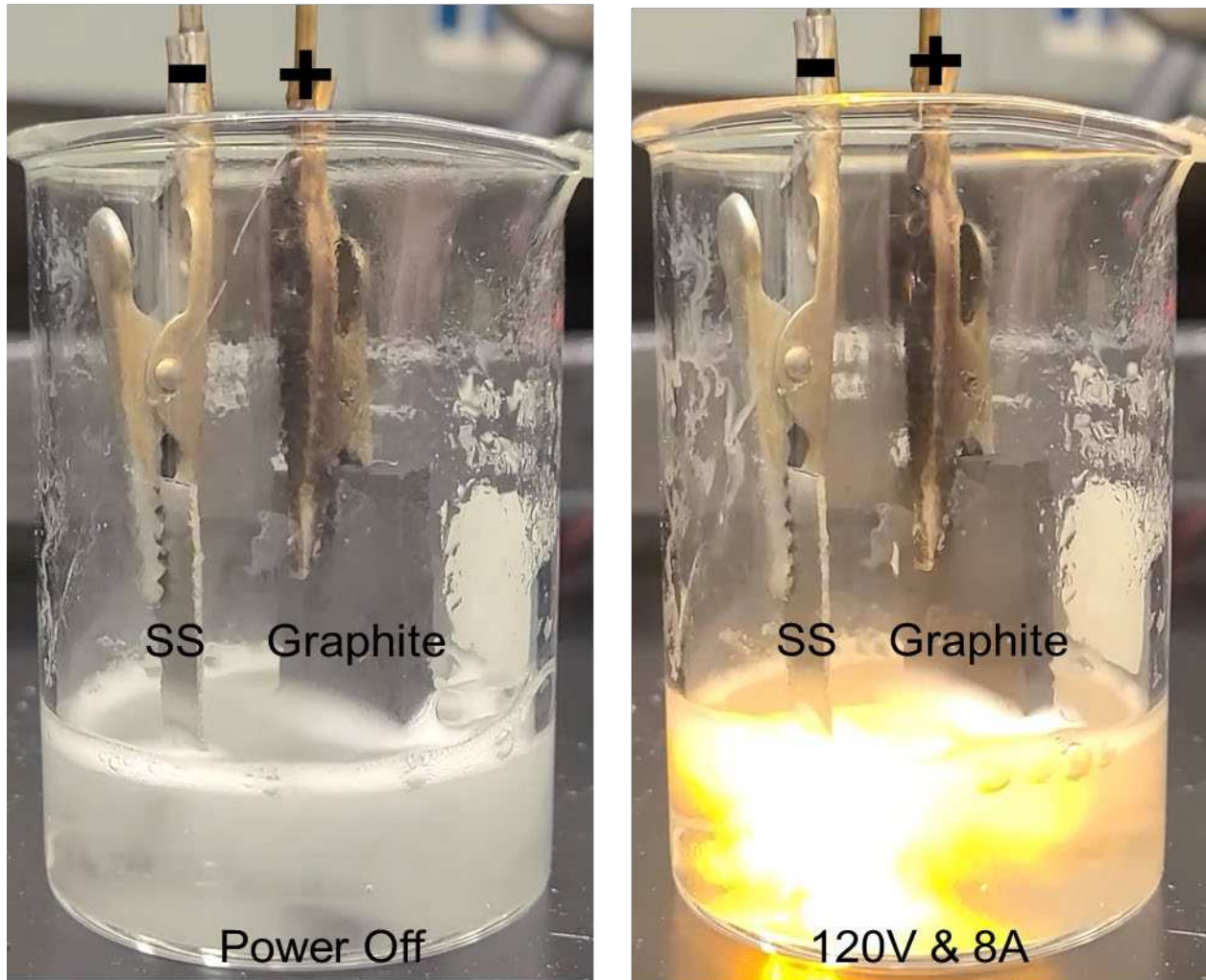


Figure 2.3.2 Images of the PEO 1 second pulse process being conducted with no power and DC power of 120V and 8A.

The difference in PEO times of 225 seconds for SS 1s and 195 seconds for SS 0.5s was due to the program cycle counting at 0. This difference in PEO times was found after characterization had been completed for SS 1s and SS 0.5s. The PEO processes for SS 1s and SS 0.5s were successful at fabricating a surface without visible graphite

deposition. The PEO modified surfaces show no visible differences from 316L SS (**Figure 2.3.3**).

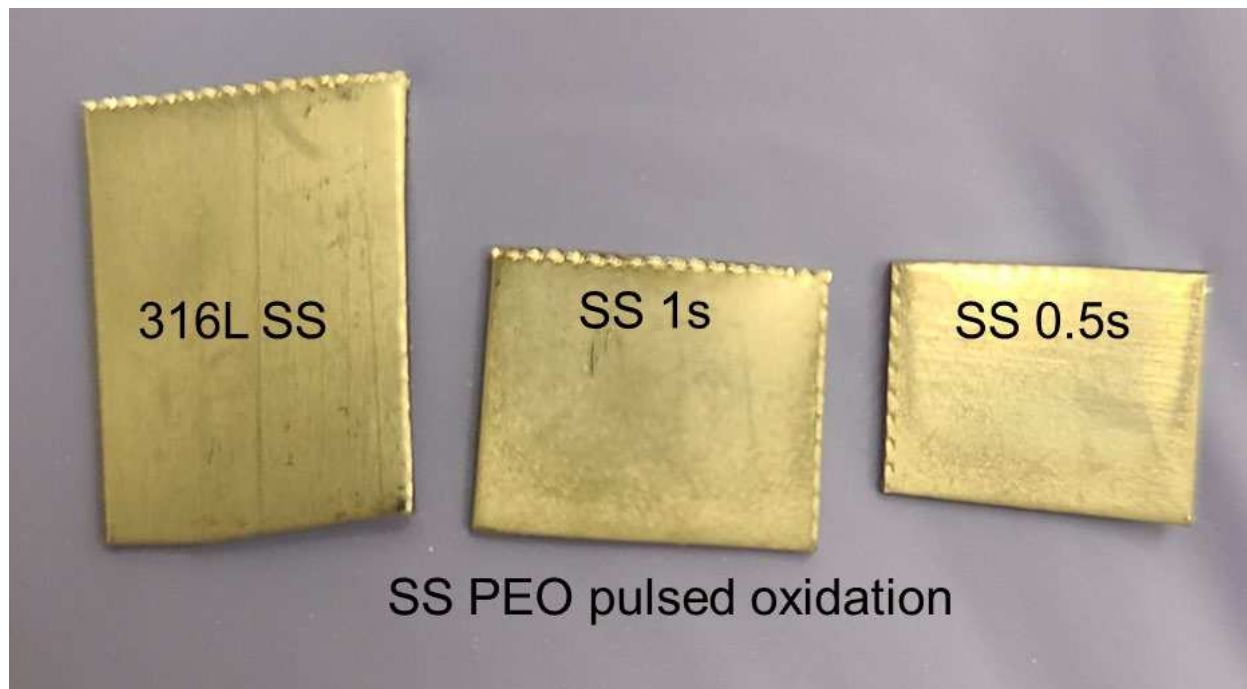


Figure 2.3.3 Images of unmodified 316L SS and PEO SS pulsed at 1 second and 0.5 second time cycles.

2.3.3 Characterization of Plasma Electrolytic Oxidized 316L Stainless Steel Surfaces

PEO SS surfaces were characterized by surface texture via SEM, surface wettability via contact angle goniometry, surface chemistry via XPS, and surface crystallinity via XRD.

SEM was utilized to characterize the surface morphology of PEO and 316l ss surfaces (**Figure 2.3.4**). 316L SS (SS) is shown to have a granular structure with no notable features within the grains themselves. SS that underwent a 1 second pulse

duration for PEO (SS 1s) and SS that underwent a 0.5 second pulse duration for PEO (SS 0.5s) show that the granular structures underwent a uniform oxidation based on the granular distribution of the surface. The PEO process fabricated peaks and valleys within the grains on the surface, thus creating a unique surface on for SS 1s and SS 0.5s when compared to SS. There were no notable differences between SS 1s and SS 0.5s in terms of the distribution of the peaks and valleys.

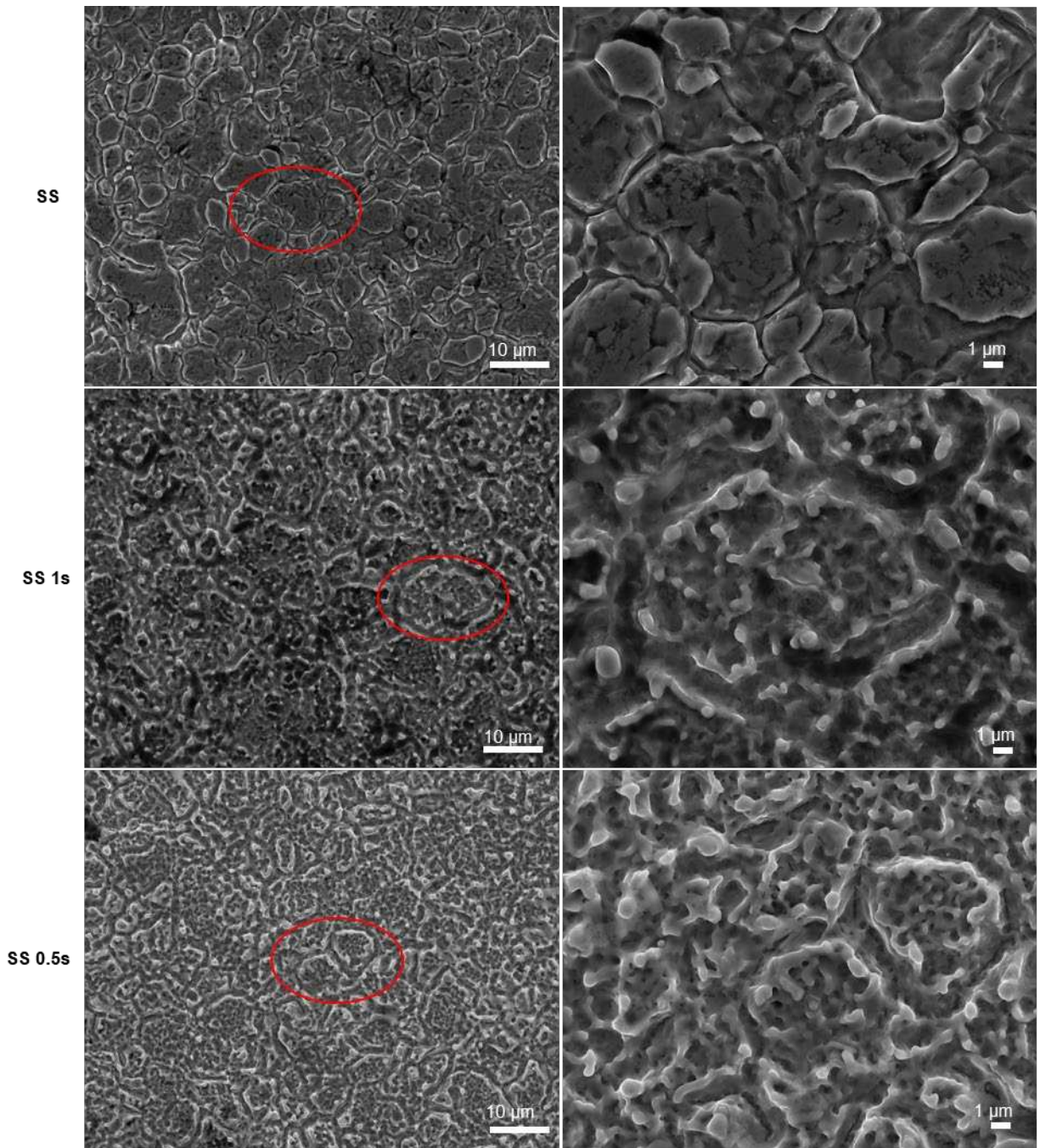


Figure 2.3.4 SEM images of the different surface at different magnifications (1500x and 5000x). The red circles indicate where the 5000x images were taken.

Contact angle measurements were utilized to characterize the wettability of the surfaces with DI water. The contact angle will demonstrate how hydrophobic or

hydrophilic a surface is, this knowledge will give insights into how the surface will affect the adhesion of mammalian cells and, along with the adhesion of bacteria. The contact angle of a surface is dependent on several surface characteristics including surface morphology, area, energy, and polarity. Contact angles indicate whether a surface is hydrophobic or hydrophilic by the angle contact that form when a droplet is placed on a surface. An angle greater than 90° indicates a hydrophobic surface while an angle less than 90° indicates a hydrophilic surface. Results show showed a significant difference of $p \leq 0.001$ for the differences in contact angle for each surface type (**Figure2.3.5**). The SS 0.5s had the most hydrophilic surface of the treatment groups with an average contact angle of approximately 70° for DI water, while SS 1s was less hydrophilic than 0.5s SS with a contact angle of approximately 81° for DI water. SS was hydrophobic with a contact angle of approximately 94° for DI water. These results demonstrate that the PEO process created a hydrophilic surface.

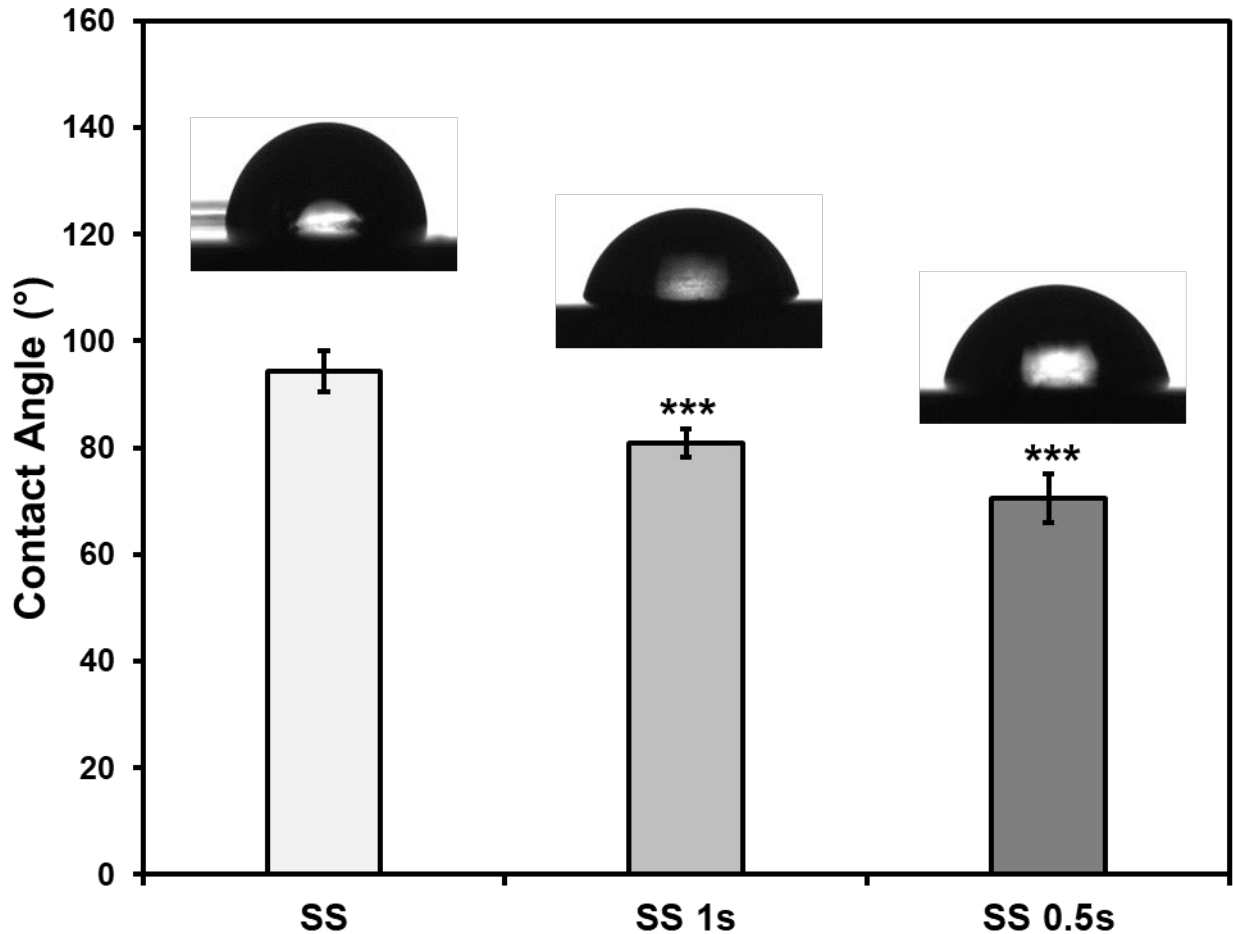


Figure 2.3.5 Contact angles of DI water (10 μ L) droplets on the different surfaces. Significant differences of (***) indicates $p \leq 0.001$ for contact angles. Error bars represent the standard deviation.

XPS was utilized to characterize the surface chemistry of the different surfaces. Knowledge of the chemical composition of the surface is vital as it may influence cellular properties such as adhesion, proliferation, etc. Survey spectra were collected peaks of Carbon (C1s), Oxygen (O1s OKLL) Calcium (Ca2p3), Iron (Fe 2p3 & 3p), and Sodium (Na 1s) were identified. The survey spectra showed large peaks at O1s and C1s for all the surfaces. The largest concentration element was carbon for all the surfaces being greater than 50%. Oxygen was the second most abundant element present on the

surfaces, greater than 12% for all surfaces. Iron concentrations were different for the surfaces with SS 1s having the highest concentration at 7.05%. Sodium was detected on the surface of SS 0.5s at 2.90%. Trace elements of Cesium, Chromium, and Tellurium were detected on the surfaces of SS 1s and SS 0.5s (**Table 1**). The high levels of Carbon present on the surfaces were partially due to known contamination within the XPS chamber. The presence of sodium on the SS 0.5s surface may be due to insufficient of the surface cleaning after the PEO process. These results demonstrate that the surface chemistry may have a role in changing the wettability of the SS 1s and SS 0.5s surfaces. The presence of Sodium on SS 0.5s may explain the difference in wettability when compared to SS 1s.

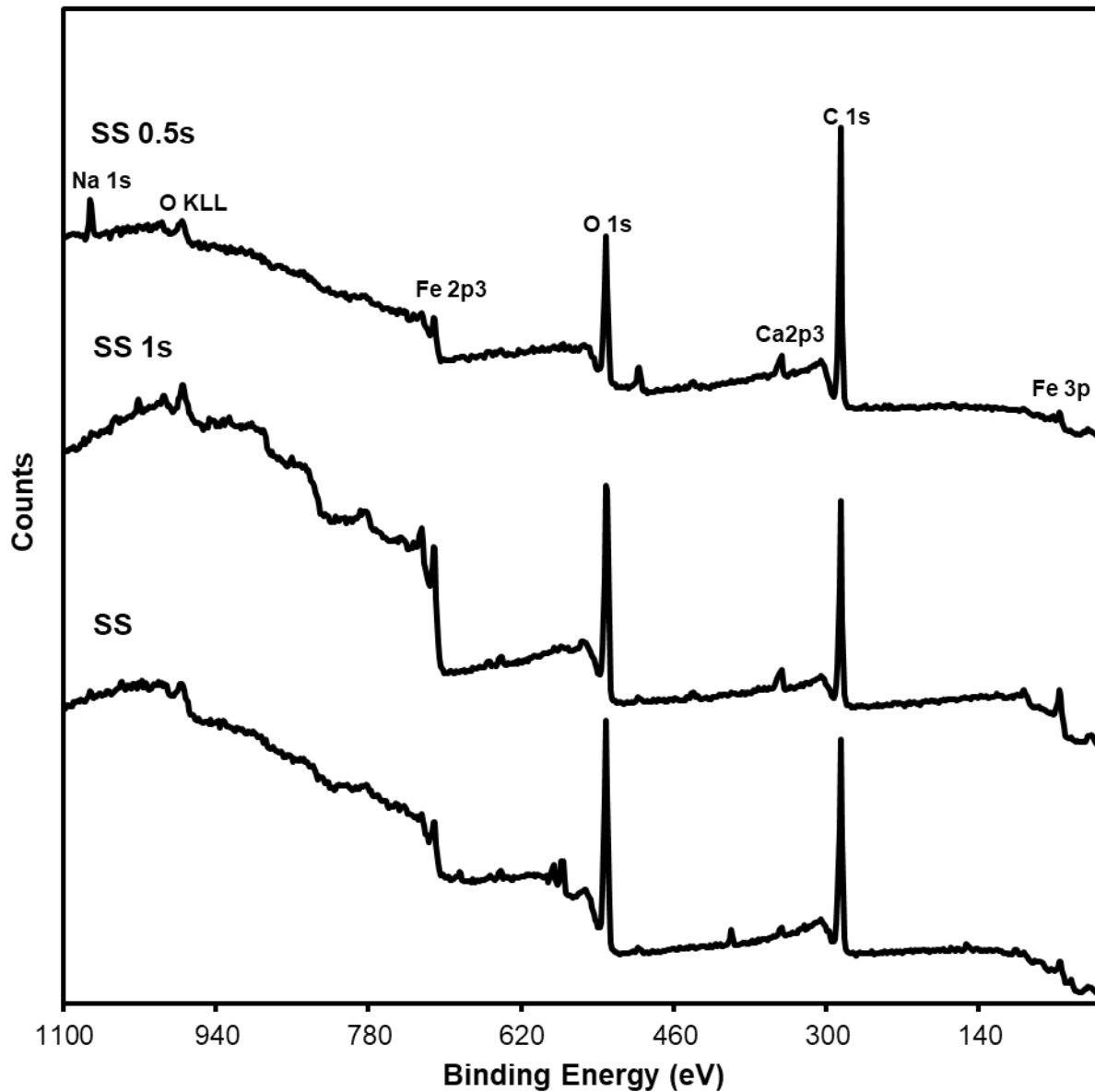


Figure 2.3.6 XPS survey scans of the different surfaces. Survey spectra was run from 1100eV to 0eV with a pass energy of 187.75eV.

Table 1: XPS elemental composition calculated from survey scans of the different surfaces.

Elements Sample	O 1s	C 1s	Ca 2p	Fe 2p	Cs 3d	Cr 2p	Te 3d	Na 1s
SS	12.76	85.85	1.28	0.1	0	0	0	0
SS 1s	31.76	57.62	1.44	7.05	1.87	0.21	0.06	0
SS 0.5s	20.03	71.69	1.24	3.16	0.08	0.84	0.02	2.96

XRD was utilized to characterize the surface crystallinity of the different surfaces (**Figure 2.3.7**). Surface crystallinity has a role in the wettability of a surface. The surfaces have notable peaks at 43°, 50.6°, and 74.4°, which relates to austenite phases of 111, 200, and 220. Austenite is the gamma phase of iron which the prevalent crystallinity of SS. These austenite phases demonstrate that PEO process did not affect the crystallinity of the surfaces. With these austenite phases remaining intact the surfaces of SS 1s and SS 0.5s will still be resistant to corrosion with intact grains. These results demonstrate that the difference in wettability for SS 1s and SS 0.5s is not due to the crystallinity.

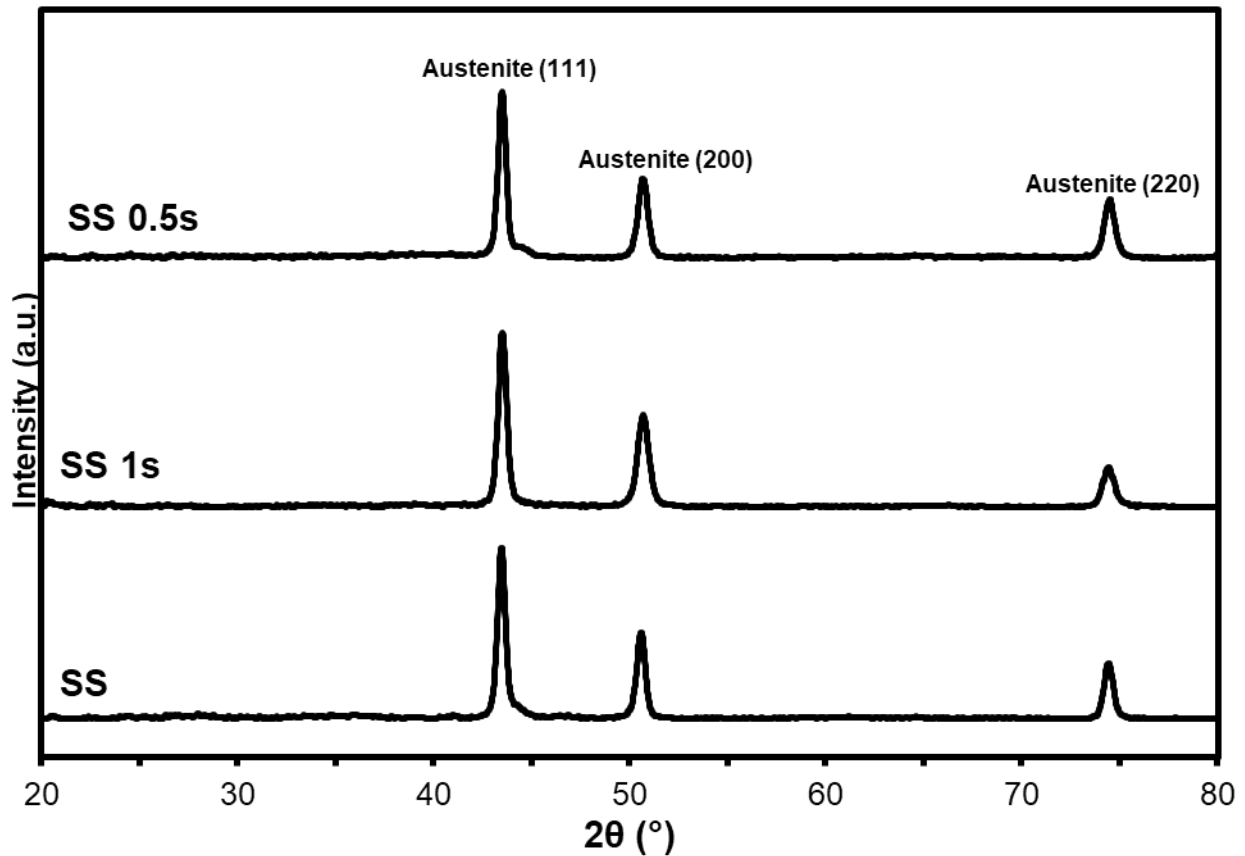


Figure 2.3.7 XRD scans of the different ss surfaces. XRD scans were collected in the 2θ range.

2.4 Conclusions

PEO modification yields a unique surface morphology that has increased hydrophilicity based on the PEO parameters used. The surface chemistry and crystallinity remained similar leading to the finding that the difference in wettability is attributed to the differences in surface morphology. Together these results demonstrate that the PEO process on 316L SS was successful in fabricating a unique surface morphology that has a unique wettability.

REFERENCES

- [1] C. Rungsiyakull, Q. Li, G. Sun, W. Li, M. Swain, Surface morphology optimization for osseointegration of coated implants, *Biomaterials*, (2010), 31, 7196-7204, <https://doi.org/10.1016/j.biomaterials.2010.05.077>.
- [2] Ball, M., Grant, D.M., Lo, W.-J. and Scotchford, C.A., The effect of different surface morphology and roughness on osteoblast-like cells. *J. Biomed. Mater. Res.*, (2008), 86A: 637-647. <https://doi.org/10.1002/jbm.a.31652>
- [3] Tuson HH, Weibel DB. Bacteria–surface interactions. *Soft matter*. (2013) ;9(17):4368-80. <https://doi.org/10.1039/C3SM27705D>
- [4] Simchen, F.; Sieber, M.; Kopp, A.; Lampke, T. Introduction to Plasma Electrolytic Oxidation—An Overview of the Process and Applications. *Coatings*, (2020), 10, 628. <https://doi.org/10.3390/coatings10070628>
- [5] M. Sumita, T. Hanawa, S.H. Teoh, Development of nitrogen-containing nickel-free austenitic stainless steels for metallic biomaterials—review, *Materials Science and Engineering: C*, (2004) 24, 6–8, 753-760, <https://doi.org/10.1016/j.msec.2004.08.030>.
- [6] R. Alias, R. Mahmoodian, K. Genasan, K.M. Vellasamy, M. Shukor, T. Kamarul, Mechanical, antibacterial, and biocompatibility mechanism of PVD grown silver–tantalum-oxide-based nanostructured thin film on stainless steel 316L for surgical applications, *Materials Science and Engineering: C*, (2020), 107, 110304, <https://doi.org/10.1016/j.msec.2019.110304>.

- [7] J. Walczak, F. Shahgaldi, F. Heatley, *In vivo* corrosion of 316L stainless-steel hip implants: morphology and elemental compositions of corrosion products. *Biomaterials*, (1998), 19, 229-237, [https://doi.org/10.1016/S0142-9612\(97\)00208-1](https://doi.org/10.1016/S0142-9612(97)00208-1).
- [8] M.H Fathi, M Salehi, A Saatchi, V Mortazavi, S.B Moosavi, In vitro corrosion behavior of bioceramic, metallic, and bioceramic–metallic coated stainless steel dental implants, *Dental Materials*, (2003), 19, 3, 188-198, [https://doi.org/10.1016/S0109-5641\(02\)00029-5](https://doi.org/10.1016/S0109-5641(02)00029-5).
- [9] D. Pathote, D. Jaiswal, V. Singh, C.K. Behera, Optimization of electrochemical corrosion behavior of 316L stainless steel as an effective biomaterial for orthopedic applications, *Materials Today: Proceedings*, (2022), 57, 1, 265-269, <https://doi.org/10.1016/j.matpr.2022.02.501>.
- [10] Aliya Bekmurzayeva, Wynter J. Duncanson, Helena S. Azevedo, Damira Kanayeva, Surface modification of stainless steel for biomedical applications: Revisiting a century-old material, *Materials Science and Engineering: C*, (2018), 93, 2018, 1073-1089, <https://doi.org/10.1016/j.msec.2018.08.049>.
- [11] A. Menezes, I. Souza, T. Costa, T. Costa, R. Sousa, R. Nascimento, M. Aires, M. Feitor, Study of the deposition of hydroxyapatite by plasma electrolytic oxidation (PEO) in stainless steel AISI 316LVM samples, *Journal of Materials Research and Technology*, 18, (2022), 1578-1589, <https://doi.org/10.1016/j.jmrt.2022.03.011>

CHAPTER 3

ADIPOCYTE DERIVED STEM CELLS ADHESION AND VIABILITY, AND OSTEOINTERGRATION ON PLASMA ELECTROLYTIC OXIDIZED 316L STAINLESS STEEL

3.1 Introduction

In vitro cell behavior on biomaterials is fundamental to understanding the *in vivo* response of a biomaterial [1]. It is essential for biomaterials of implantable devices to provide a suitable environment for cells to adhere and proliferate, while also not causing overreactive response from the adaptative and innate immune system [2]. Hydrophilic surfaces have been shown to enhance cell adhesion [3]. In this work, Adipocyte derived stem cells (ADSCs) were cultured on the surfaces of 316L SS, and the PEO modified surfaces of SS 1s and SS 0.5s. Cell studies were separated into two parts the initial adhesion and viability, and osteointegration. The initial adhesion and viability of ADSCs was characterized using fluorescence microscopy, scanning electron microscopy, and cellular viability assay of Alamar blue. Osteointegration was characterized using fluorescence microscopy, scanning electron microscopy, alkaline phosphatase assay, and a calcium deposition assay.

3.2 Methods and materials

3.2.1 Adipocyte derived stem cell culture on Plasma Electrolytic Oxidized 316L Stainless Steel Surfaces

Adipocyte derived stem cells (ADSCs) were isolated from adipose tissue by Prof. Cox-York's laboratory at Colorado State University. The procedures were conducted in compliance with the National Institutes of Health's "Guiding Principles for Ethical Research". ADSCs at passage 3 were cultured in minimum essential media (MEM) (α -MEM, HyClone™) with 10% v/v fetal bovine serum along with 1% v/v penicillin & streptomycin at 37°C and 5% CO₂. The media was changed every 48 hrs until the cells reached confluency. Prior to culturing the cells on different surfaces, they were sterilized in a 48-well plate with 70% ethanol for 15 mins, rinsed three times with phosphate-buffered saline (PBS), and exposed to ultra-violet (uv) light for 30 mins. The cells were diluted to a concentration of 10,000 ADSCs per/ml and 0.3 ml of this solution was placed on sterilized surfaces. The cells were cultured in an incubator at 37°C and 5% CO₂ for the entire duration of the study.

3.2.2 Adipocyte derived stem cell adhesion and proliferation on Plasma Electrolytic Oxidized 316L Stainless Steel Surfaces

The viability of ADSCs on different surfaces was characterized by commercially available Alamar Blue assay (Invitrogen). After days 1, 4, and 7 days of culture, the 300 μ l of media was mixed with 30 μ l of assay reagent and incubated at 37°C for 6 hrs. The absorbance of the solution was measured at 570 nm and 600 nm in a microplate reader (FLUOstar Omega, BMG Lab tech). The viability was calculated as described in the assay

protocol. ADSCs seeded in wells without any surfaces were used as positive control and wells with just media were used as negative control.

The adhesion and proliferation of ADSCs on the surfaces was characterized using fluorescence microscopy. After 1, 4, and 7 days of cell culture, the cells adhered on different surfaces were fixed with 3.7% formaldehyde in PBS for 15 mins, followed rinsing 3 times with PBS for 5 mins each. The fixed cells on different surfaces were permeabilized with 1% Triton X-100 solution in PBS for 3 mins, followed by rinsing 2 times with of PBS for 5 mins each. The fixed and permeabilized cells were then stained by incubating the surfaces in rhodamine phalloidin solution (70 nM, Cytoskeleton) for 20 mins, followed incubating them in DAPI solution (300 nM, ThermoFisher Scientific) for 5 mins in a dark environment. The stain solution was aspirated, and the surfaces were rinsed 3 times with PBS for 5 mins each. The surfaces were imaged via fluorescence microscope (Zeiss).

Morphology of cells on different surfaces was characterized after days 1, 4, & 7 of cell culture via SEM. Adhered ADSCs on the surfaces were fixed via glutaraldehyde fixative for 45 minutes, followed by sodium cacodylate buffer for 10 minutes, followed by sequential rinses of 35%, 50%, 70%, & 100% ethanol for 10 minutes each. After 100% ethanol removal, the surfaces were allowed to air dry and placed in a desiccator until imaging. The surfaces were coated with 10nm of gold before being imaged at 15kV under SEM using 1500X and 5000X magnification.

3.2.3 Adipocyte derived stem cell differentiation and osteointegration on Plasma Electrolytic Oxidized 316L Stainless Steel Surfaces

After Day 7 of initial culture cell culture, osteogenic differentiation was induced by adding 1% v/v of dexamethasone, 2% v/v of ascorbic acid, and 6% v/v of β -glycerol phosphate in the culture media. The differentiation media was changed every 48 hours for 21 days.

After 7 and 21 days (week 1 and week 3) of differentiation cell culture, the surfaces were rinsed once with PBS. Surfaces were incubated in TritonX-100 (0.2% v/v in DI water) for 20 minutes at 100 rpm. The supernatant was removed and was stored in the freezer for Micro BCA and ALP activity assays.

A Micro BCA assay kit (Thermo Scientific) was used to quantify the total amount of protein content on the surfaces. 150 μ l of supernatant (0.2% Triton X-100 solution with protein extracted) was mixed with 150 μ l of working reagent and incubated for 2 hrs at 37 °C in a dark environment, followed by the measurement of absorbance at 562 nm. The results for the total amount of protein were determined via a standard absorbance curve obtained previously using the manufacturer's guidelines.

The ALP content of the adhered ADSCs on the surfaces was characterized After one and three weeks of differentiation culture. A colorimetric assay kit (QuantiChrom™, BioAssay Systems) was used to determine the ALP activity on the surfaces. 50 μ l of the supernatant (0.2% Triton X-100 solution with protein extracted) was mixed with 150 μ l of working reagent. The absorbance was measured at 405 nm after 0 and 4 mins and the ALP activity was obtained following the manufacturer's guidelines. The ALP activity was normalized to the total protein content on each surface.

The calcium deposition on the surfaces was characterized after one and three weeks of differentiation culture. Calcium deposition was determined by a calcium reagent set (Teco Diagnostics). After supernatant removal, the surfaces were dried and incubated in 6 N HCl solution for 2 hours to dissolve the deposited calcium. After that, 20 μ l of the acid-calcium solution was collected from each well and mixed with 1 ml of working reagent prepared following the manufacturer's protocol. The absorbance of the acid-calcium solution was read at 570 nm and the calcium concentration was calculated using the manufacturer's guidelines. The calcium concentration was normalized to total protein content on each surface.

Cellular osteocalcin expression on the surfaces was characterized via fluorescence microscopy using immunofluorescent staining. After one and three weeks of differentiation culture the same protocol as in section (3.2.2) was followed to fix and permeabilize cells. The surfaces were placed in bovine serum albumin (BSA) solution (10% v/v in PBS) for 30 mins to block non-specific binding sites. After that, the substrates were incubated with osteocalcin primary antibody solution (1:100 in 1% BSA) for 60 mins, followed by three rinses with PBS. The substrates were then placed in secondary antibody-FITC solution (1:200 in 1% BSA) for 45 mins. After rinsing with PBS, the substrates were stained with DAPI and rhodamine phalloidin and imaged as detailed in section 3.2.2.

Cellular morphology on the surfaces was characterized after via SEM. Adhered ADSCs on the surfaces were fixed via glutaraldehyde fixative for 45 minutes, followed by sodium cacodylate buffer for 10 minutes, followed by sequential rinses of 35%, 50%, 70%, & 100% ethanol for 10 minutes each. After 100% ethanol removal, the surfaces were

allowed to air dry and placed in a desiccator until imaging. The surfaces were coated with 10nm of gold before being imaged at 15kV under SEM, using 1500X and 5000X.

3.2.4 Statistical Analysis

Characterization of cellular adhesion was conducted using 3 different samples per surface using 3 different locations, repeated twice (n=18) for days 1, 4, and 7. Characterization of osteocalcin coverage was conducted using 3 different samples per surfaces using 3 different locations repeated twice (n=18) for week 1 and week 3. Tukey tests were conducted for quantitative comparisons. An alpha value 0.05 was used and p-values ≤ 0.05 were considered statistically significant. R software was used to conduct all analysis.

3.3 Results and Discussion

3.3.1 ADSC adhesion and viability on the different surfaces

The initial adhesion and viability of cells on to biomaterial surfaces is a key component to understanding biocompatibility [4]. It is desirable for a biomaterial surface to promote proliferation and adhesion of cells when a biomaterial is implanted [5]. Decreases in the initial adhesion and proliferation rates on implantable devices will have a delayed healing process, lack of osteointegration, and potential implant rejection [6]. Hence, it is vital to understand the initial viability of a biomaterial's surface.

Cell adhesion was characterized by utilizing fluorescence microscopy. ADSCs were able to successfully adhere to all surfaces, PEO modified surfaces had cells closer

expanding towards one another in more longer shapes for Days 1 and 4 while SS had more trapezoidal cells upon the surface. By Day 7 there was considerable growth across all surfaces (**Figure 3.3.1**).

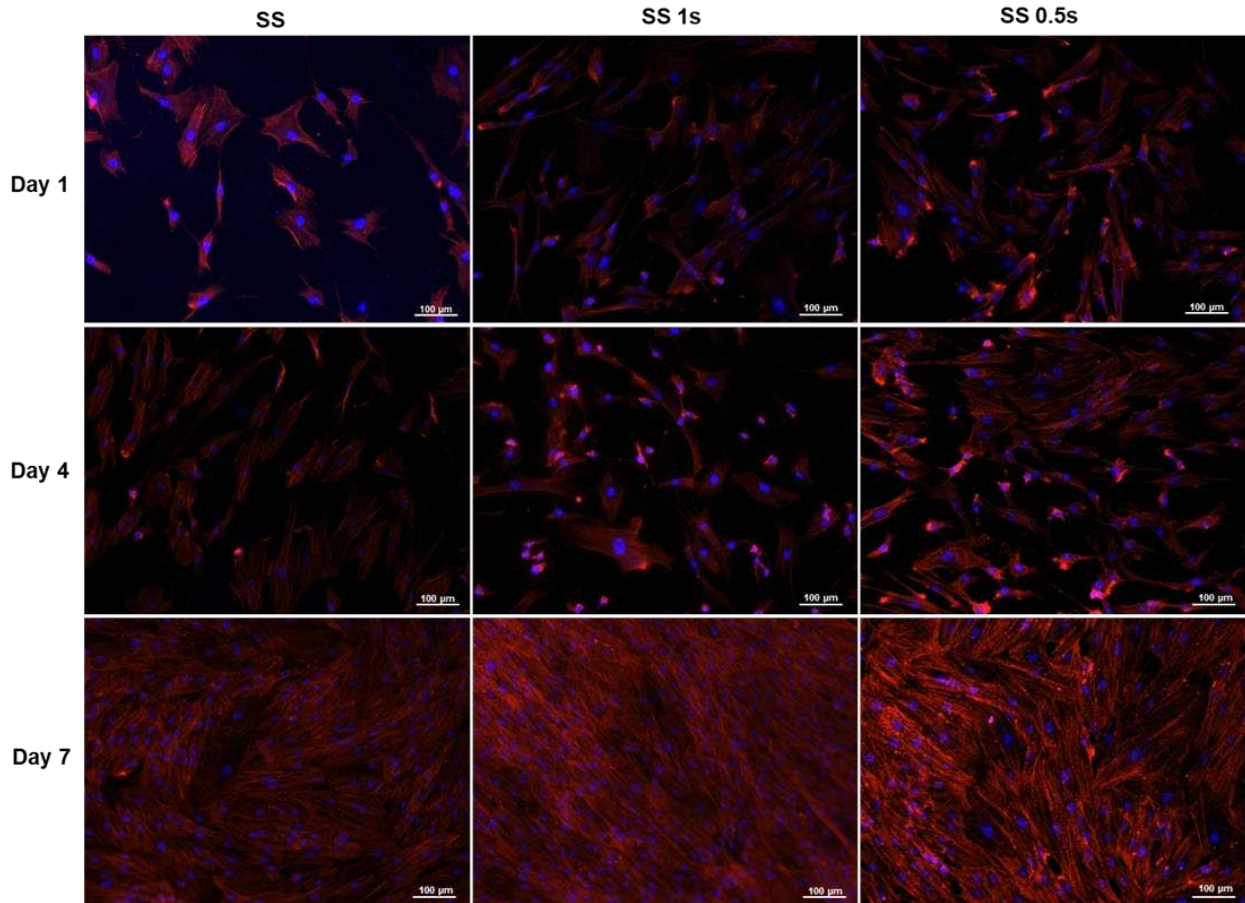


Figure 3.3.1 Fluorescence microscopy images, at 10x zoom, adhesion of day 1, 4, and 7 after incubation upon the surfaces. Cytoskeletons appear red, while nuclei appear blue under fluorescence.

When the fluorescence images were compared quantitatively for cell count there were no significant differences between the surfaces for Days 4 and 7. Days 4 and 7 were significantly different between one another for the surfaces. SS 1s had the highest average cell count for Day 7 and SS 0.5s had the highest (**Figure 3.3.2**).

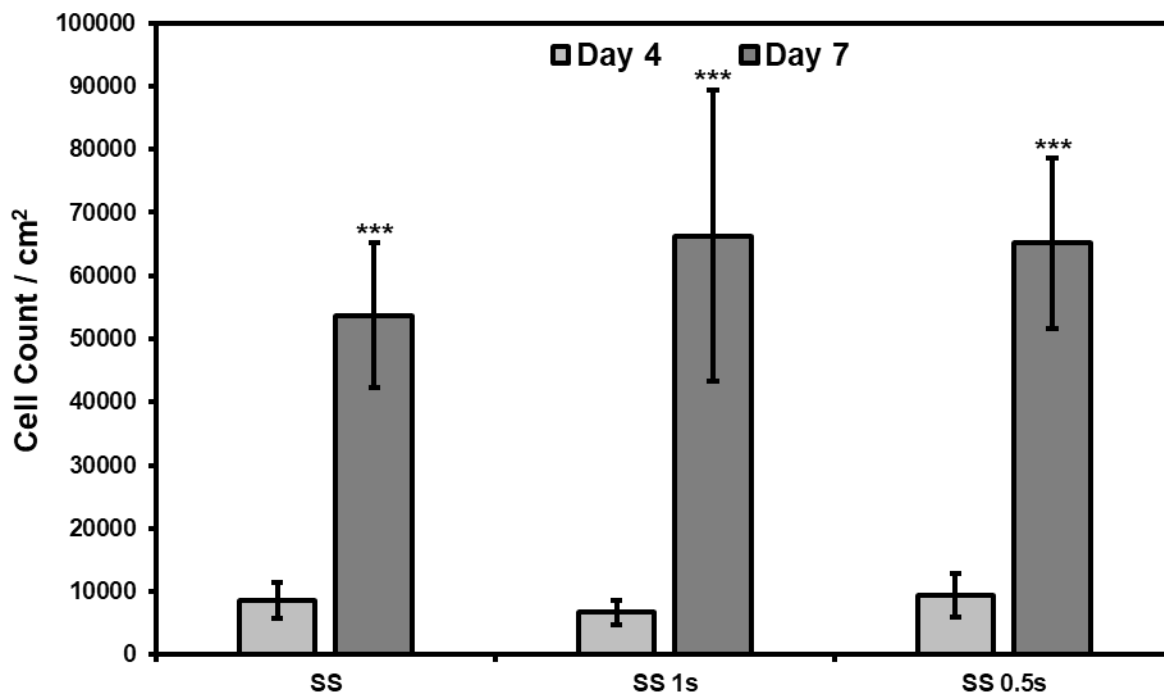


Figure 3.3.2 Cell counts quantitative comparison. Significant differences of (***) indicates $p \leq 0.001$ for Cell count per cm^2 . Error bars represent the standard deviation.

A similar result was found in the Alamar blue assay, there were no significant differences between the surfaces or with the positive control (**Figure 3.3.3**). These results demonstrate the viability of the PEO modified surfaces of SS 1s and SS 0.5s was maintained when compared to SS. These results demonstrate that PEO modification of the SS 1s and SS 0.5s did not adversely affect the initial viability or adhesion of ADSCs on the surfaces.

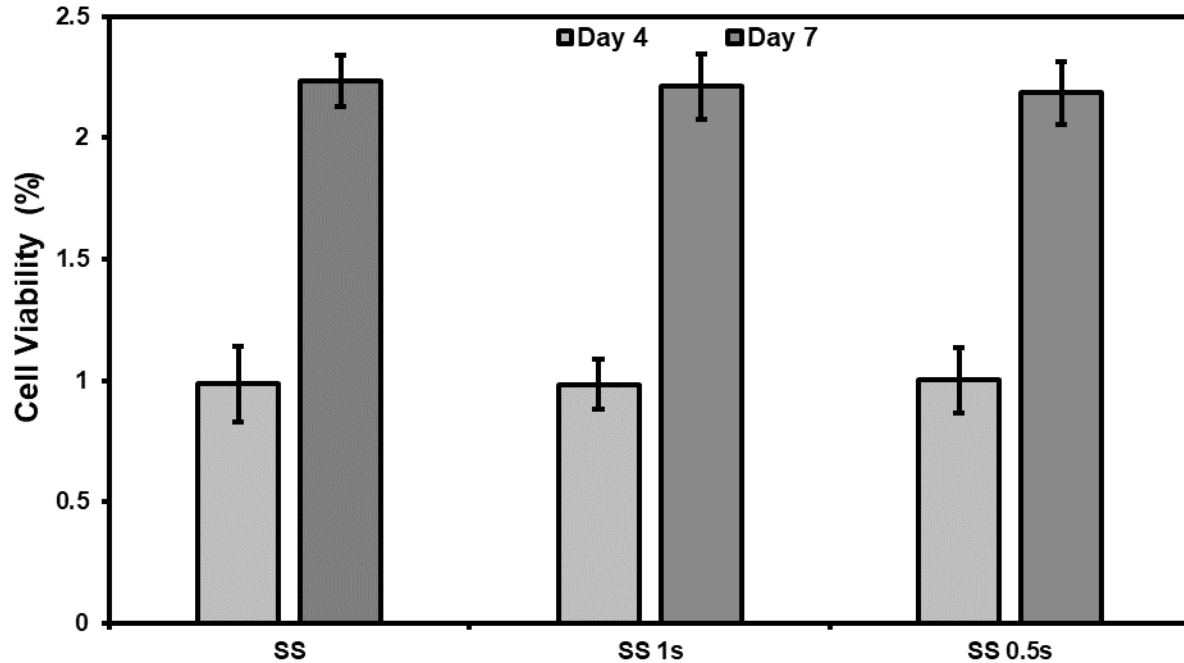


Figure 3.3.3 Cell viability, alamar blue was conducted through a plate reader determining the absorbance of the alamar blue dye at 600 and 570 nm after 6 hours of incubation. Error bars represent the standard deviation.

Results from the cellular morphology of ADSCs demonstrate similar results seen in the fluorescence microscopy. Days 1 and 4 show the cells beginning to spread out onto the surfaces and expanding filopodium onto to the surfaces. While Day 7 shows mass cell coverage upon the surfaces (**Figure 3.3.4**). Upon the imaging at a higher magnification, it can be observed that the ADSCs were forming larger filopodium expanding outwards towards other ADSCs on the surfaces (**Figure 3.3.5**).

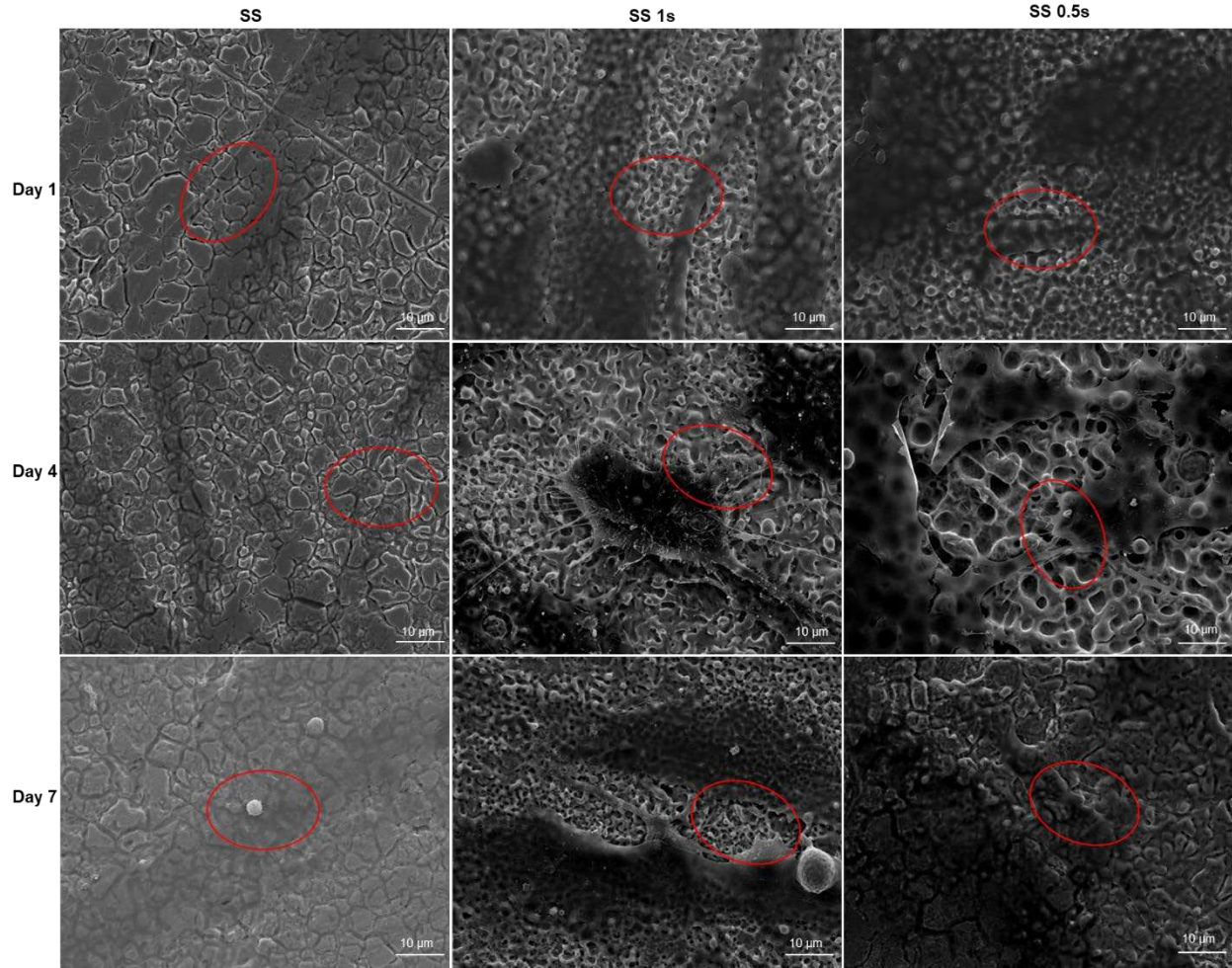


Figure 3.3.4 Representative SEM images of ADSCs on different surfaces at 1500x. The red circles represent were the 5000x images were taken from the 1500x image.

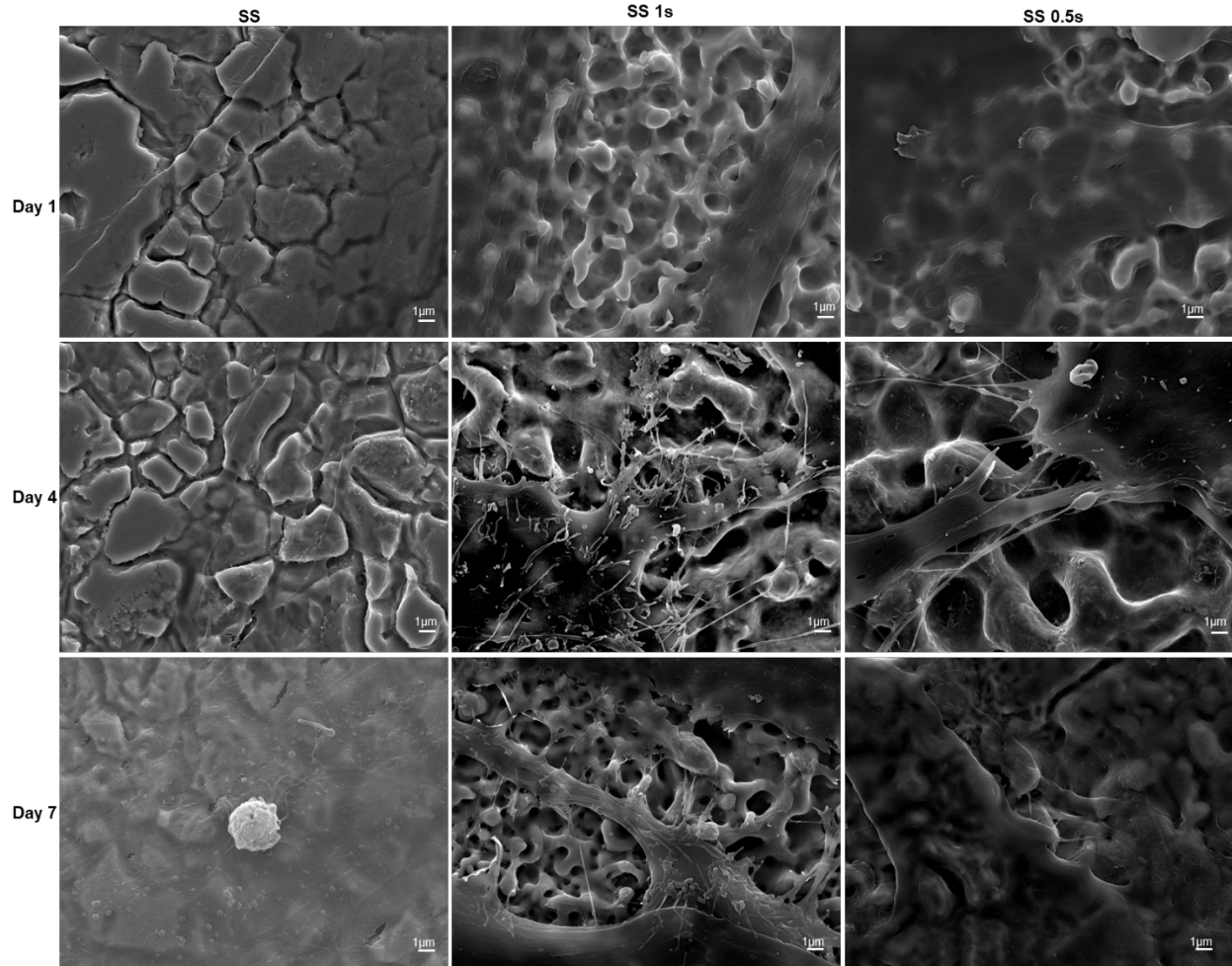


Figure 3.3.5 Representative SEM images of ADSCs on different surfaces at 5000x.

The PEO modified surfaces of SS 1s and SS 0.5s demonstrated similar viability and initial adhesion seen with the SS surfaces. Of note was the growth exponentiation of ADSCs on all the surfaces between days 4 & 7. When the morphology was of ADSCs was examined SS 1s and SS 0.5s had notable increases of filopodium.

3.3.2 Osteointegration of ADSCs on the different surfaces

Osteo integration of cells into biomaterials is an important aspect of biocompatibility [7]. ADSCs are pluripotent and have potential to be differentiated into osteoblasts [4,8]. Osteoblasts are cells with the primary role of forming new bone tissue [9]. Alkaline phosphatase (ALP) is an enzyme responsible for dephosphorylating a phosphate based monoester with water into an alcohol and phosphate [10]. It has been shown that ALP levels will be increased during bone formation as the enzyme is a by product of osteoblasts [10]. Hydroxyapatite is the bioavailable available of calcium phosphate in mammalian tissue. Hydroxyapatite present in collagenous matrices of bone tissue, and is estimated to be 50% to 70% of the weight of bone [11]. The role of hydroxyapatite is bind to provide support to bone by binding to calcium ions, thus being the source of calcium in bone tissue [11]. Calcium is the primary structural component of bone that provides the strength for the tissue [11]. The most abundant noncollagenous protein excreted by osteoblasts is osteocalcin [12]. Osteocalcin has several roles including, but not limited to endocrine signaling to the pancreas for insulin regulation and eventual ossification into bone tissue [12]. Osteocalcin has been known as an indicator of bone and concentrations have been shown to be directly related to levels of bone formation [12]. These markers demonstrate how well cells are differentiated and how the well osteointegration occurred on the surfaces. The following section examines how at how ADSCs differentiated into osteoblasts and how they were able to deposit materials to form bone tissue in, alkaline phosphatase, calcium deposition, and osteocalcin after 1 and 3 weeks of differentiation.

The results of the ALP assay demonstrates that the concentration was the highest in week 1 (**Figure 3.3.6**). SS 0.5s had the highest concentration of ALP at week 1, which is positively related to the osteocalcin coverage seen in week 3 on the surface. SS had the lowest ALP concentration which follows with the osteocalcin coverage seen for that surface.

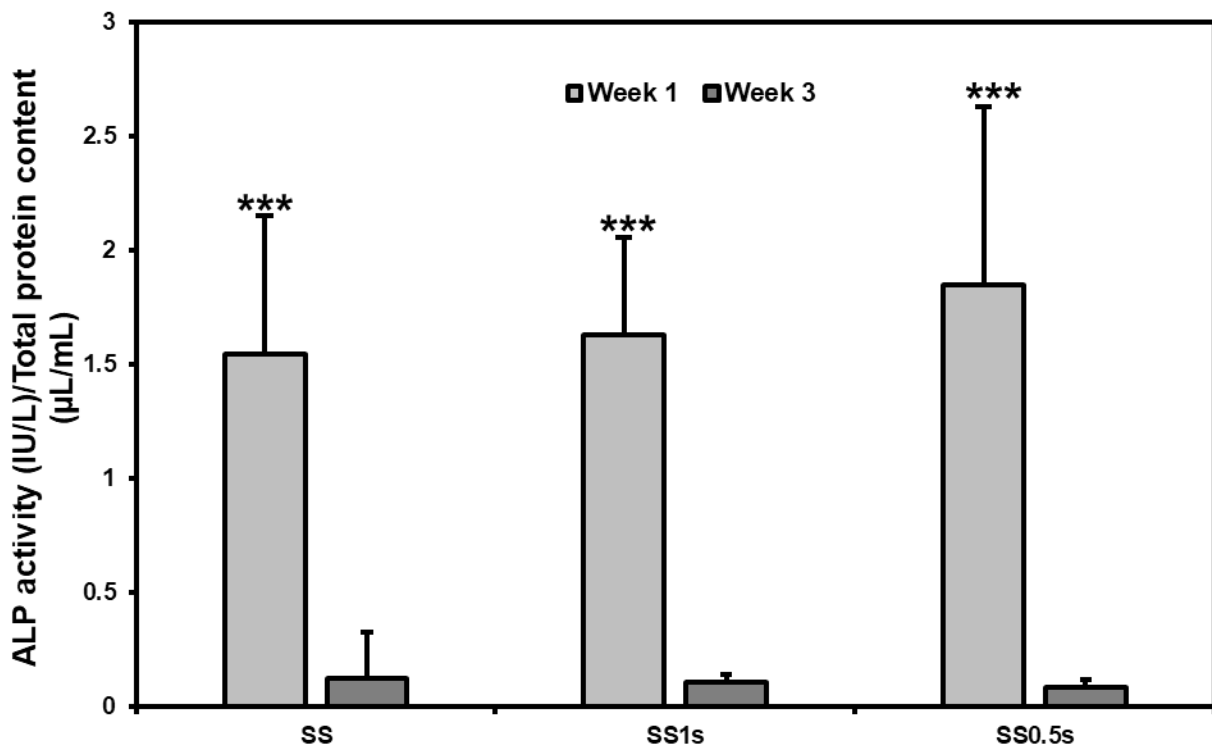


Figure 3.3.6 Alkaline phosphatase assay quantitative comparison between the different surfaces. Significant differences of (***) indicates $p \leq 0.001$ for ALP content per total protein content. Error bars represent the standard deviation.

The results from the calcium deposition assay demonstrate that the concentration was the highest in week 3 for all the surfaces (**Figure 3.3.7**). These results follow what has been seen in the osteocalcin coverage and ALP results. There were no significant

different differences between the surfaces at week 1 or week 3. SS 0.5s had the highest calcium concentration. SS followed similar trends seen in ALP and osteocalcin coverage results with having lower concentrations at week 3.

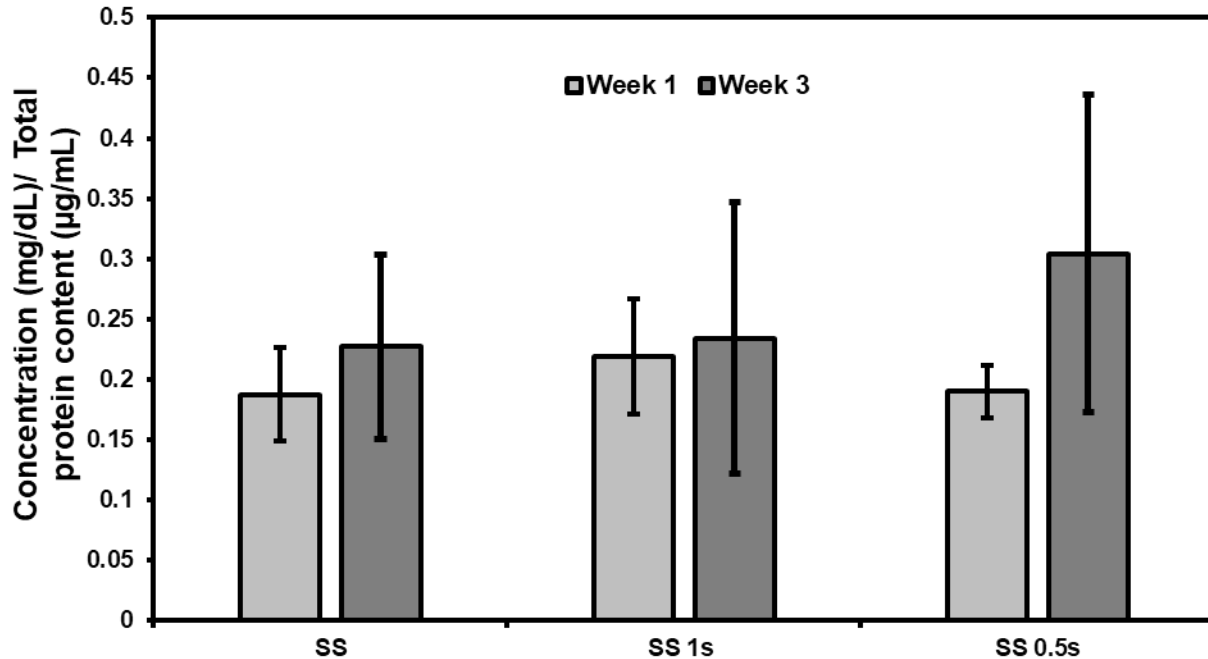


Figure 3.3.7 Calcium deposition assay quantitative comparison. Significant differences of (***) indicates $p \leq 0.001$) for Calcium concentration per total protein content Error bars represent the standard deviation.

Osteocalcin coverage was characterized by utilizing fluorescence microscopy. After one week of differentiation, ADSCs were able to differentiate and deposit osteocalcin upon the surface. Differences between week 1 and week 3 can be seen in the fluorescent images, with week 3 having higher deposition than week 1 for all surfaces. There are no notable differences between the surfaces at week 1 or week 3 (**Figure3.3.6**).

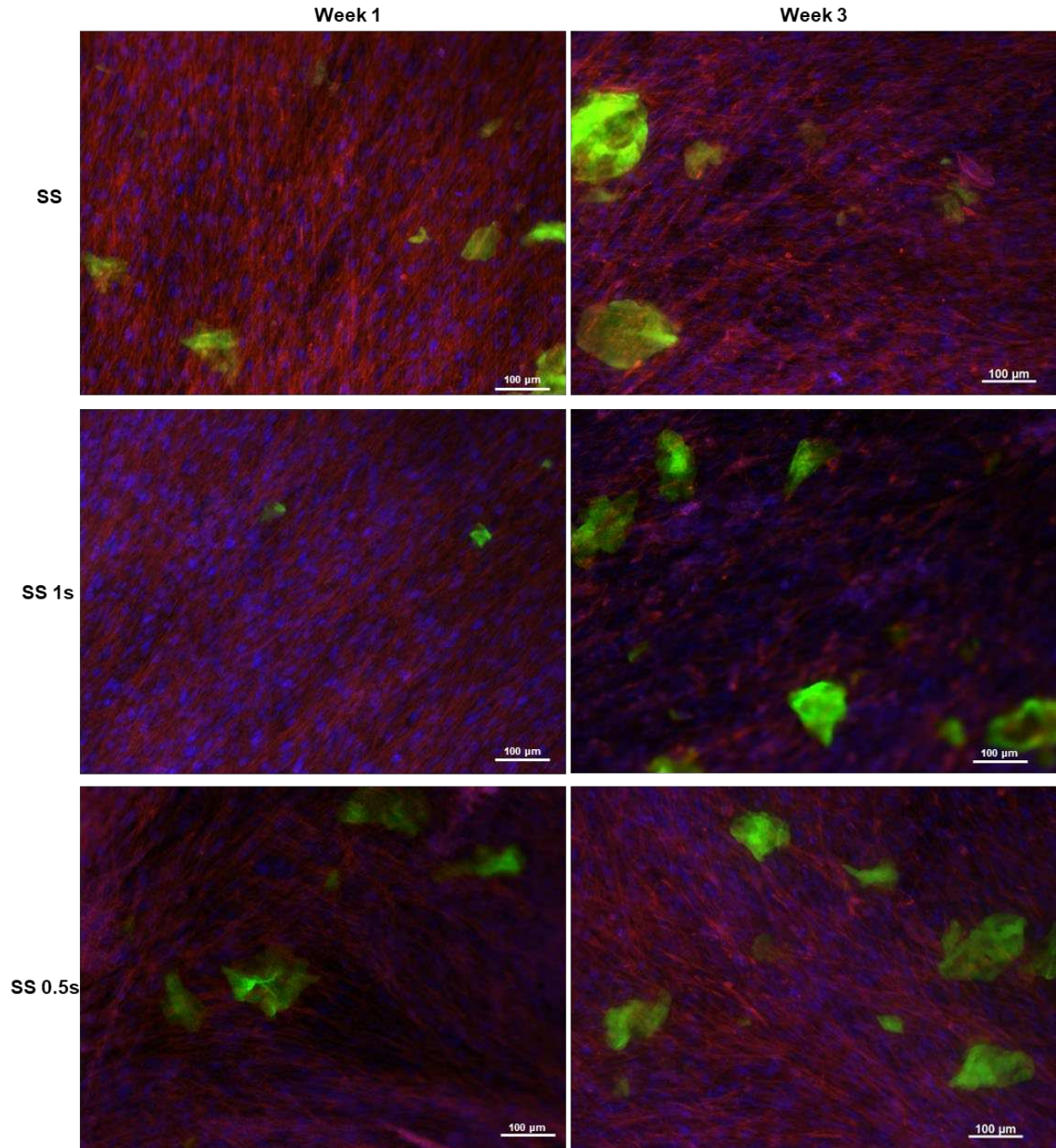


Figure 3.3.8 Osteocalcin fluorescence images Fluorescence microscopy images, at 10x zoom, adhesion of week 1 and week 3 after incubation upon the surfaces. Cytoskeletons appear red, nuclei appear blue under fluorescence, while osteocalcin deposits appear green.

Quantitative analysis results of osteocalcin coverages confirmed what can be seen in the fluorescent images. There was a statistical difference between week 1 and week 3 for all surfaces. When the surfaces were compared to one another the results demonstrated that there was no statistical difference between the surfaces (**Figure 3.3.7**). Of interest was the difference between SS and the PEO modified surfaces at week 1 and then week 3. SS had the highest osteocalcin at week 1, however, at week 3 SS had the lowest osteocalcin coverage. SS 0.5s had a coverage of 6.03% a 1.5% increase over SS. SS 1s had the lowest osteocalcin coverage in week 1 by week 3 it had coverage greater than SS.

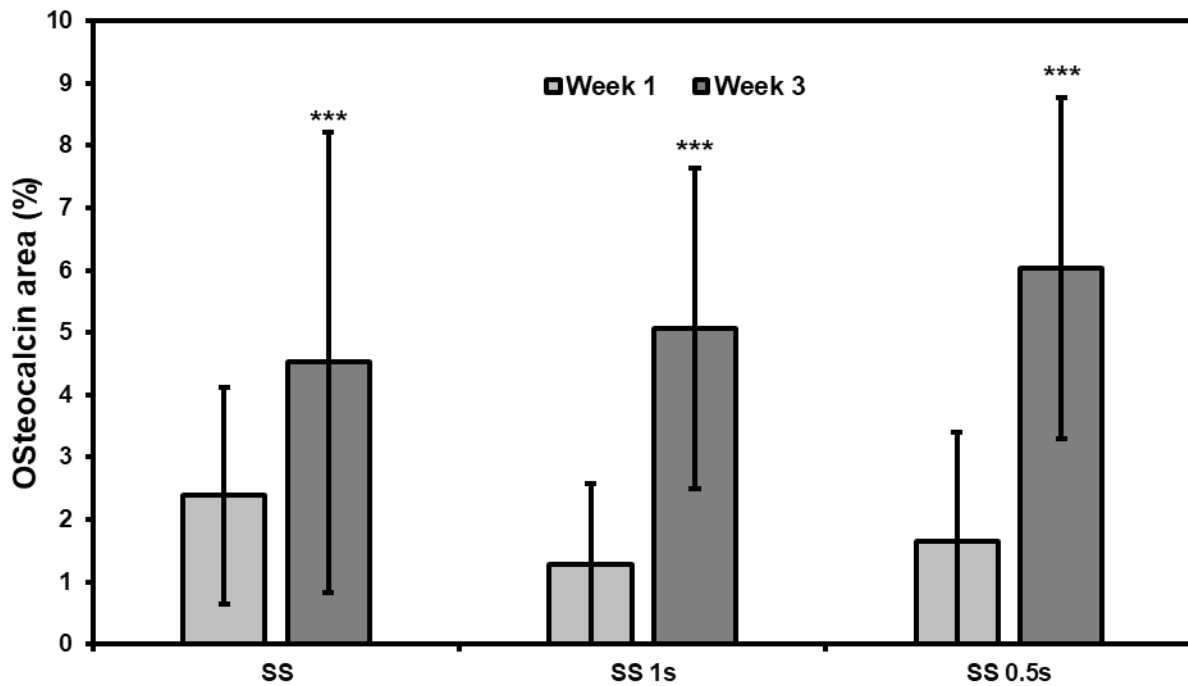


Figure 3.3.9 Osteocalcin coverage quantitative comparison. Significant differences of (***) indicates $p \leq 0.001$) for osteocalcin area coverage percentages. Error bars represent the standard deviation.

SEM images demonstrate similar results seen in the fluorescence microscopy. With little osteocalcin deposition at week 1 and a noticeable increase at week 3 (**Figure 3.3.8**). Upon higher magnification it can be seen how cells upon the surface are interacting with the deposited materials (**Figure 3.3.9**). By week 1 the cells had formed a mass coverage of the surfaces. After week 3, the differentiation cells had begun depositing materials on the surfaces. The morphology indicated that the differentiation cells on the PEO modified surfaces of SS 1s and SS 0.5s maintained the osteointegration capability when compared to SS.

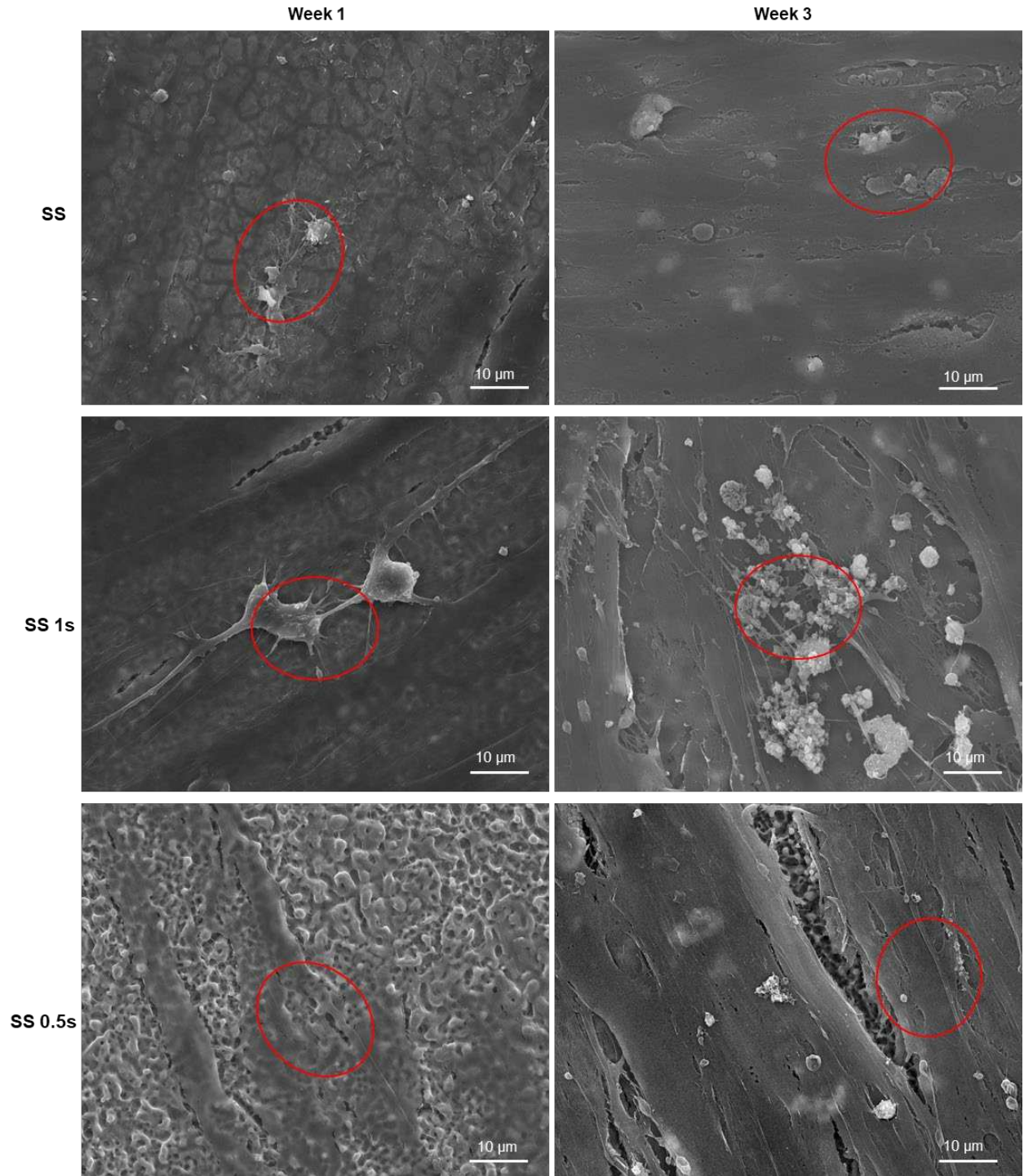


Figure 3.3.10 Cell differentiation morphology SEM images 1500x. Red circles indicate where the 5000x images were taken.

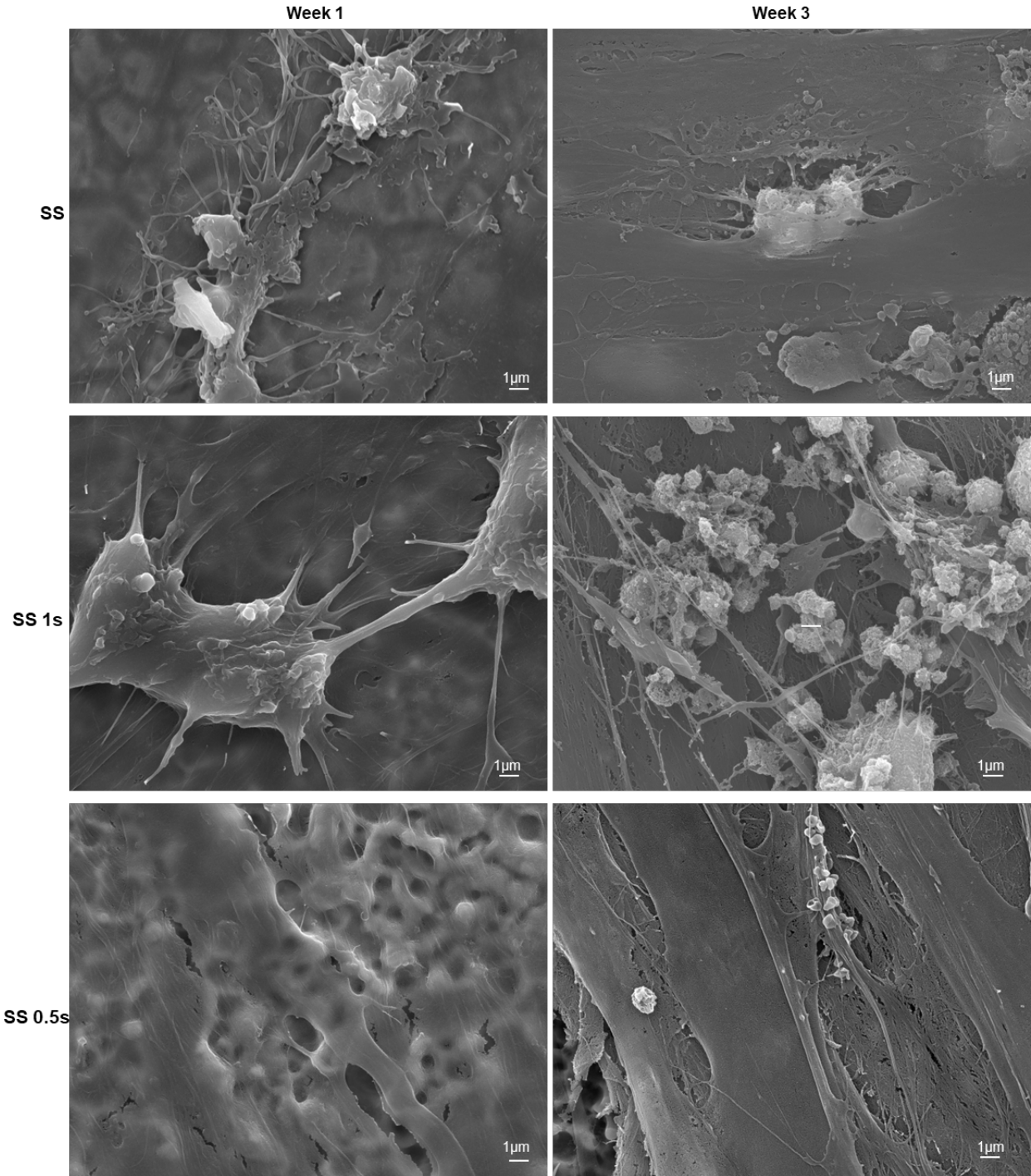


Figure 3.3.11 Representative SEM images of ADSCs on different surfaces at 5000x.

Overall, these results demonstrate that there was successful differentiation and osteointegration for the surfaces. The differences between the PEO surfaces and 316L

were noticeable. However, they did not prove to be significantly different. The lack of statistical significance between these surfaces may be due to the differences in wettability not being great enough to enhance the initial cellular adhesion.

3.4 Conclusions

The results demonstrate the PEO modified surfaces maintain the cellular response of ADSCs when compared to 316L SS. While it has been shown that hydrophilic surfaces enhance cellular adhesion, the hydrophilicity of SS 1s and SS0.5s was not enough to show a significant difference in adhesion or osteointegration for ADSCs. However, SS 0.5s surface had the highest coverage of osteocalcin, which relates to the higher concentrations of ALP seen in week 1 and the higher concentration of calcium concentration seen in week 3. The difference while not statistically significant may be attributable to the difference seen in wettability for the SS 0.5s surface, as more hydrophilic surfaces are shown to enhance cellular adhesion.

REFERENCES

- [1] Cowden, K., Dias-Netipanyj, M.F. & Popat, K.C. Adhesion and Proliferation of Human Adipose-Derived Stem Cells on Titania Nanotube Surfaces. *Regen. Eng. Transl. Med.* (2019), 5, 435–445, <https://doi.org/10.1007/s40883-019-00091-9>
- [2] Sundararaj, K, & Bangaru, M., In Vitro Biocompatibility Study on Stainless Steel 316L After Nano Finishing, *Proceedings of the ASME 2017 International Mechanical Engineering Congress and Exposition*, (2017) Volume 3: Biomedical and Biotechnology Engineering. Tampa, Florida, USA. November 3–9, <https://doi-org.ezproxy2.library.colostate.edu/10.1115/IMECE2017-72606>
- [3] Anwar IB, Santoso A, Saputra E, Ismail R, Jamari J, Van der Heide E., Human Bone Marrow-Derived Mesenchymal Cell Reactions to 316L Stainless Steel: An in Vitro Study on Cell Viability and Interleukin-6 Expression, *Adv Pharm Bull*, (2017), 7(2), 335-338, doi: 10.15171/apb.2017.040.
- [4] Roberta M. Sabino, Gabriela Mondini, Matt J. Kipper, Alessandro F. Martins, Ketul C. Popat, Tanfloc/heparin polyelectrolyte multilayers improve osteogenic differentiation of adipose-derived stem cells on titania nanotube surfaces, *Carbohydrate Polymers*, (2021), 251, 117079, <https://doi.org/10.1016/j.carbpol.2020.117079>.
- [5] Popat, K.C., Chatvanichkul, K.-I., Barnes, G.L., Latempa, T.J., Jr., Grimes, C.A., and Desai, T.A., Osteogenic differentiation of marrow stromal cells cultured on nanoporous alumina surfaces., *J. Biomed. Mater. Res.*, (2007), 80A: 955-964. <https://doi.org/10.1002/jbm.a.31028>

[7] Renata Francielle Bombaldi de Souza, Fernanda Carla Bombaldi de Souza, Andrea Thorpe, Diego Mantovani, Ketul C. Popat, Ângela Maria Moraes, Phosphorylation of chitosan to improve osteoinduction of chitosan/xanthan-based scaffolds for periosteal tissue engineering, *International Journal of Biological Macromolecules*, (2020), 143, 619-632, <https://doi.org/10.1016/j.ijbiomac.2019.12.004>.

[8] Karim Bordjih, Jean-Yves Jouzeau, Didier Mainard, Elisabeth Payan, Jean-Pierre Delagoutte, Patrick Netter, Evaluation of the effect of three surface treatments on the biocompatibility of 316L stainless steel using human differentiated cells, *Biomaterials*, (1996), 17, 5, 491-500, [https://doi.org/10.1016/0142-9612\(96\)82723-2](https://doi.org/10.1016/0142-9612(96)82723-2).

[9] Zhou, Chuan, et al., The effects of Sr-incorporated micro/nano rough titanium surface on rBMSC migration and osteogenic differentiation for rapid osteointegration., *Biomaterials science*, (2018), 1946-1961, <https://doi.org/10.1039/C8BM00473K>

[10] Elena García-Gareta, Melanie J. Coathup, Gordon W. Blunn, Osteoinduction of bone grafting materials for bone repair and regeneration, *Bone*, (2015), 81, 112-121, <https://doi.org/10.1016/j.bone.2015.07.007>.

[11] Jeong, J., Kim, J.H., Shim, J.H. et al. Bioactive calcium phosphate materials and applications in bone regeneration. *Biomaterials Research*, (2019), 23, 4, <https://doi.org/10.1186/s40824-018-0149-3>

[12] L. Di Medio, M. Brandi, Chapter Three - Advances in bone turnover markers, Editor(s): Gregory S. Makowski, *Advances in Clinical Chemistry*, Elsevier, (2021), 105, 101-140, <https://doi.org/10.1016/bs.acc.2021.06.001>.

CHAPTER 4

BACTERIAL ADHESION AND MORPHOLGY ON PLASMA ELECTROLYTIC OXIDIZED 316L STAINLESS STEEL

4.1 Introduction

Bacterial infection is a leading cause of early implant failure for endosseous dental implants, and is present orthopedic, cochlear, and other implants [1,2,3]. The opportunistic nosocomial infection of *Staphylococcus aureus* (*S. aureus*), a gram-positive bacterial species, is a common pathogen for recipients of implantable devices [4]. The prevalence of *S. aureus* in our environment is the main cause of the infection being so common, it is estimated that 30% of the human population carries *S. aureus* in their nasal passages [5]. This prevalence of *S. aureus* combined with; the increasing virulence of *S. aureus* make this bacterial species a problematic pathogen [6]. *S. aureus* has antibiotic resistant strains; these strains include MRSA and VRSA (methicillin resistant and vancomycin resistant *S. aureus*), vancomycin and methicillin are two notable antibiotics used to treat gram positive bacterial infections [7]. One way to prevent bacterial proliferation on biomaterials is through surface modification. There are various methods for modifying surfaces to be antibacterial these include: coating the surface with various ions or materials such as silver, copper, or antibiotics, changing the chemistry of the surface with polymerization or functionalization, creating surface structures on the micro and/or nanoscale as seen with bioinspired surfaces of cicada wings and shark skin [8]. Surface structure changes allow a surface to become either hydrophilic or hydrophobic

depending on the methodology used; if a surface becomes superhydrophobic it will prevent bacteria from adhering to the surface, however, if a surface becomes superhydrophilic it will create bactericidal surface [8]. In this chapter, SS and PEO modified SS were characterized for their bacterial adhesion and proliferation for *S. aureus* bacterial species after incubation of 6 and 24 hours.

4.2 Materials and Methods

4.2.1 Bacterial Culture on Plasma Electrolytic Oxidized 316L Stainless Steel Surfaces

The bacterial adhesion capability of gram-positive bacteria of the surfaces were characterized by using the bacterial species of *Staphylococcus aureus*, ATCC 6538. Bacterial cultures were obtained from agar plate culture and pellet to be grown in a liquid media culture of Tryptic Soy broth in an incubator at 37° C until the optical density at 600 nm was approximately 1. A 100 µL aliquot of the solution was taken, and the absorbance was read at 600 nm using a plate reader. The bacteria solutions were diluted to obtain a concentration of 10⁶ CFU/mL. The surfaces were then incubated in 500 µL of bacteria solution for 6 and 24 hours.

4.2.2 Characterization of Bacterial adhesion on Plasma Electrolytic Oxidized 316L Stainless Steel Surfaces

Bacterial adhesion and proliferation were characterized via fluorescence microscopy. Fluorescence microscopy was used to measure the amount of live and dead bacteria that adhered to the surfaces. After incubation for 6 and 24 hours, the bacteria solution was removed, and the surfaces were rinsed three times with PBS to remove any non-adhered bacteria. The surfaces were then incubated in stain solution (3 $\mu\text{L}/\text{mL}$ of propidium iodide and Syto 9 stain 1:1 in PBS) for 20 min at room temperature, in a dark environment. After incubation, the stain solution was aspirated, and the surfaces were rinsed once with PBS. The adhered bacteria were fixed to the surfaces using a 3.7% formaldehyde solution in PBS for 15 minutes, followed by 3 consecutive PBS rinses for 5 minutes each. The surfaces were imaged using a fluorescent microscope (Zeiss). ImageJ was used to calculate the percentage of live and dead bacteria on the surfaces.

Bacterial morphology and biofilm formation was characterized after 6 hours and 24 hours of bacterial culture via SEM. SEM followed the same procedure and imaging as detailed in section (3.2.3).

4.2.3 Statistical analysis

Characterization of bacterial adhesion was conducted using 3 different samples per surface using 3 different locations, repeated twice (n=18). Tukey tests were conducted for quantitative comparison. An alpha value 0.05 was used and p-values \leq 0.05 were considered statistically significant. R software was used to conduct all analysis.

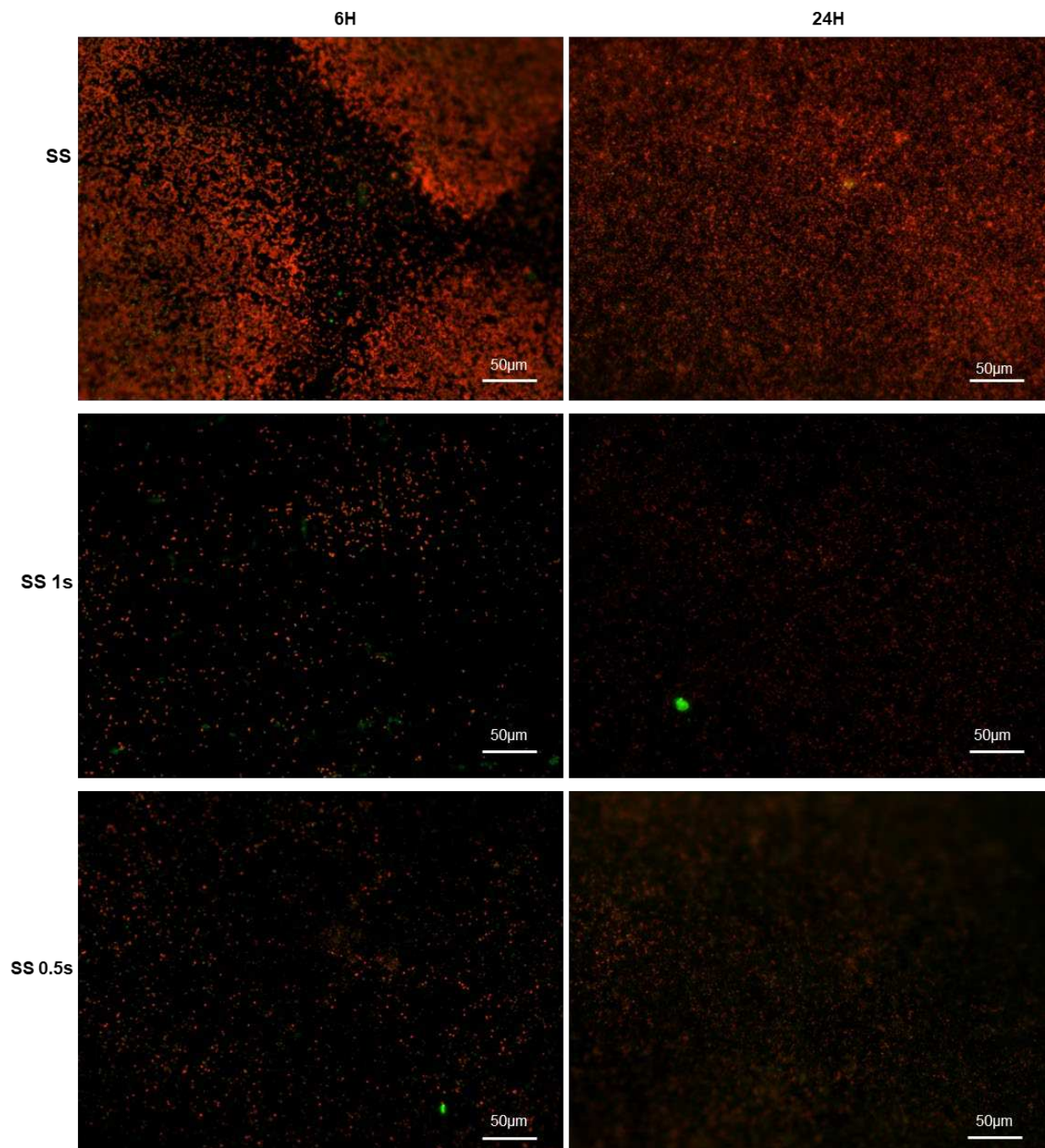
4.3 Results and Discussion

4.3.1 Bacterial adhesion and proliferation on Plasma Electrolytic Oxidized 316L Stainless Steel Surfaces

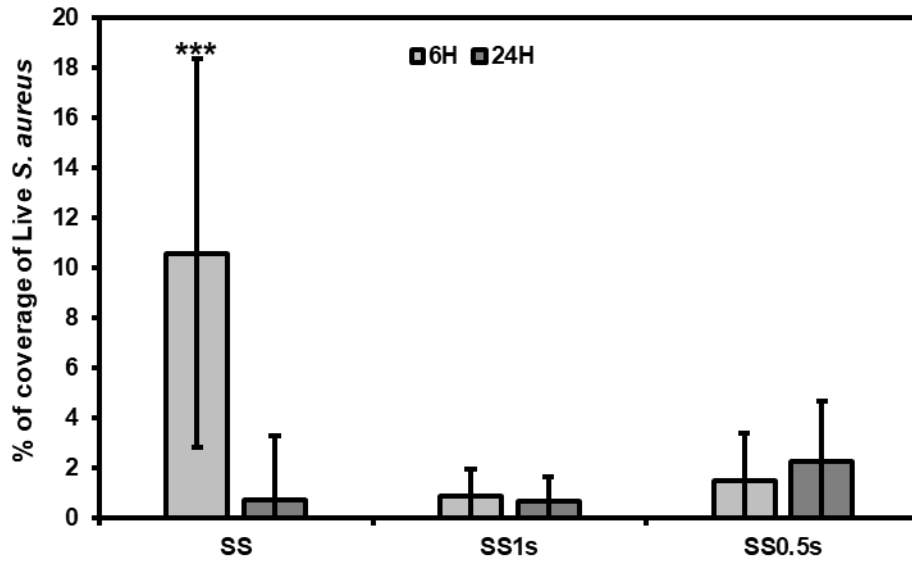
Prevention of the initial adhesion of bacteria is fundamental to preventing infections on biomaterials. It is desirable for a biomaterial's surface to limit the number of bacteria that can adhere to it. Increases in the number of bacteria adhered to a surface may lead to an infection that could delay the healing process, potentially leading to an implant failure. Hence it is vital to understand the initial adhesion of a biomaterials surface.

Fluorescence microscopy was utilized to characterize the adhesion abilities of *S. aureus* on the surfaces. A commercially available live/dead stain kit containing Syto-9 and propidium was utilized to determine the difference between live and dead bacteria that were adhered to the surfaces. Syto-9 stains living bacteria green, while propidium stains dead bacteria red when observed under fluorescence. Fluorescence images taken of *S. aureus* indicated a reduction in adhesion for SS 1s and SS 0.5s at both 6 and 24 hours (**Figure 4.3.1 A**). When the images were quantified via ImageJ and statistically tested there was a significant difference, $p \leq 0.001$, for the live bacteria at 6 hours between SS and the PEO fabricated surfaces of SS 1s and SS 0.5s (**Figure 4.3.1 B**). As well, there existed a significant difference, $p \leq 0.001$, for the dead bacteria at 24 hours between SS and the PEO fabricated surfaces of SS 1s and SS 0.5s (**Figure 4.3.1 C**). There existed no statistically significant differences between SS 1s and SS 0.5s for *S. aureus* live-dead analysis (**Figure 4.3.1 B & C**). The reduction in *S. aureus* adhesion between SS and PEO

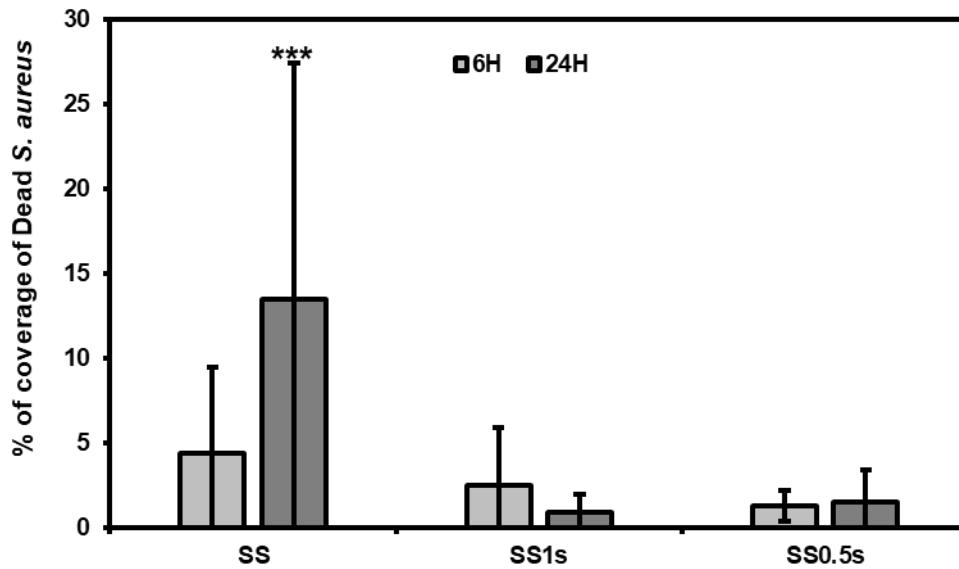
fabricated surfaces is attributable to the differences in the surface morphology creating a more hydrophilic surface.



(A)



(B)

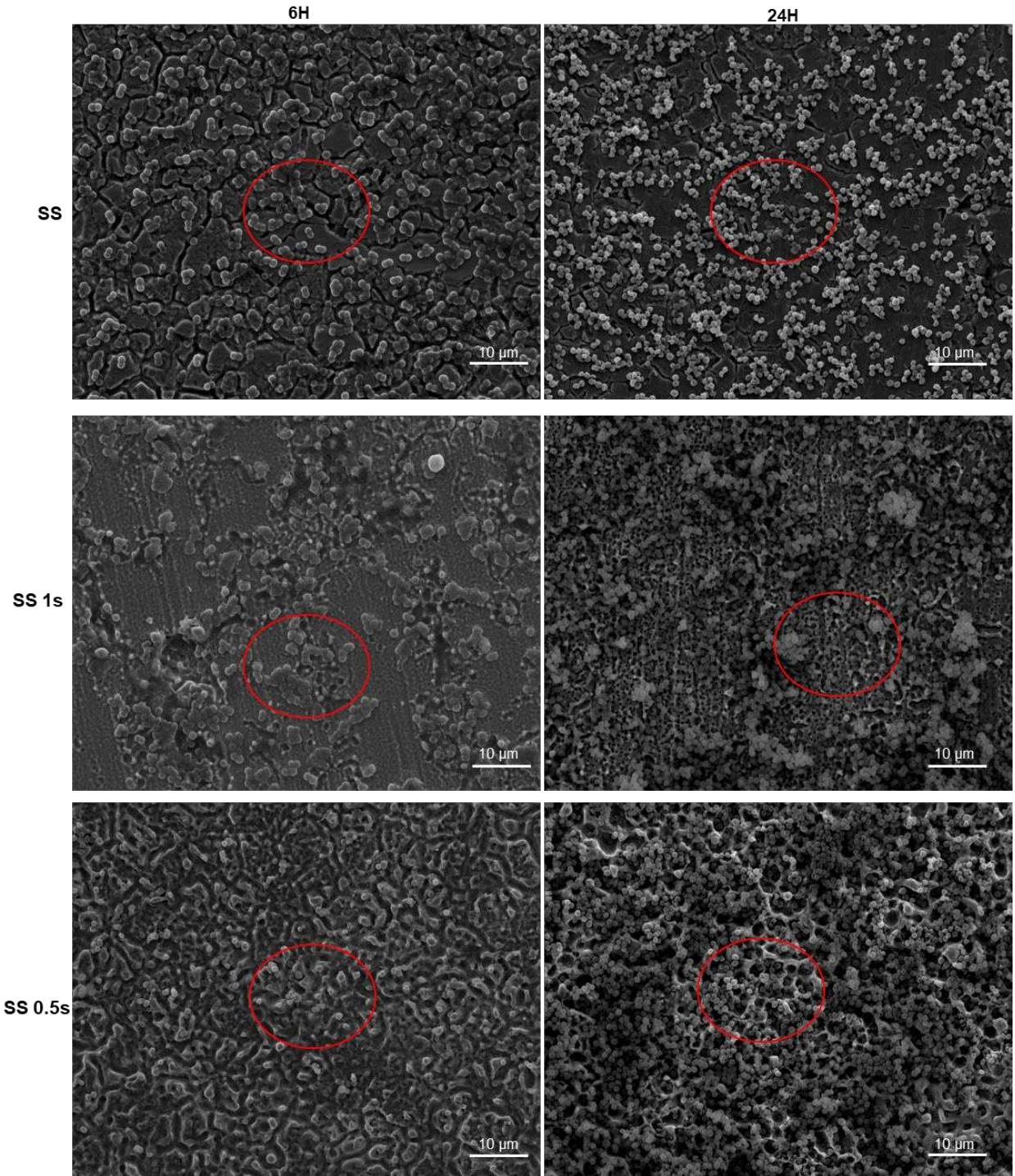


(C)

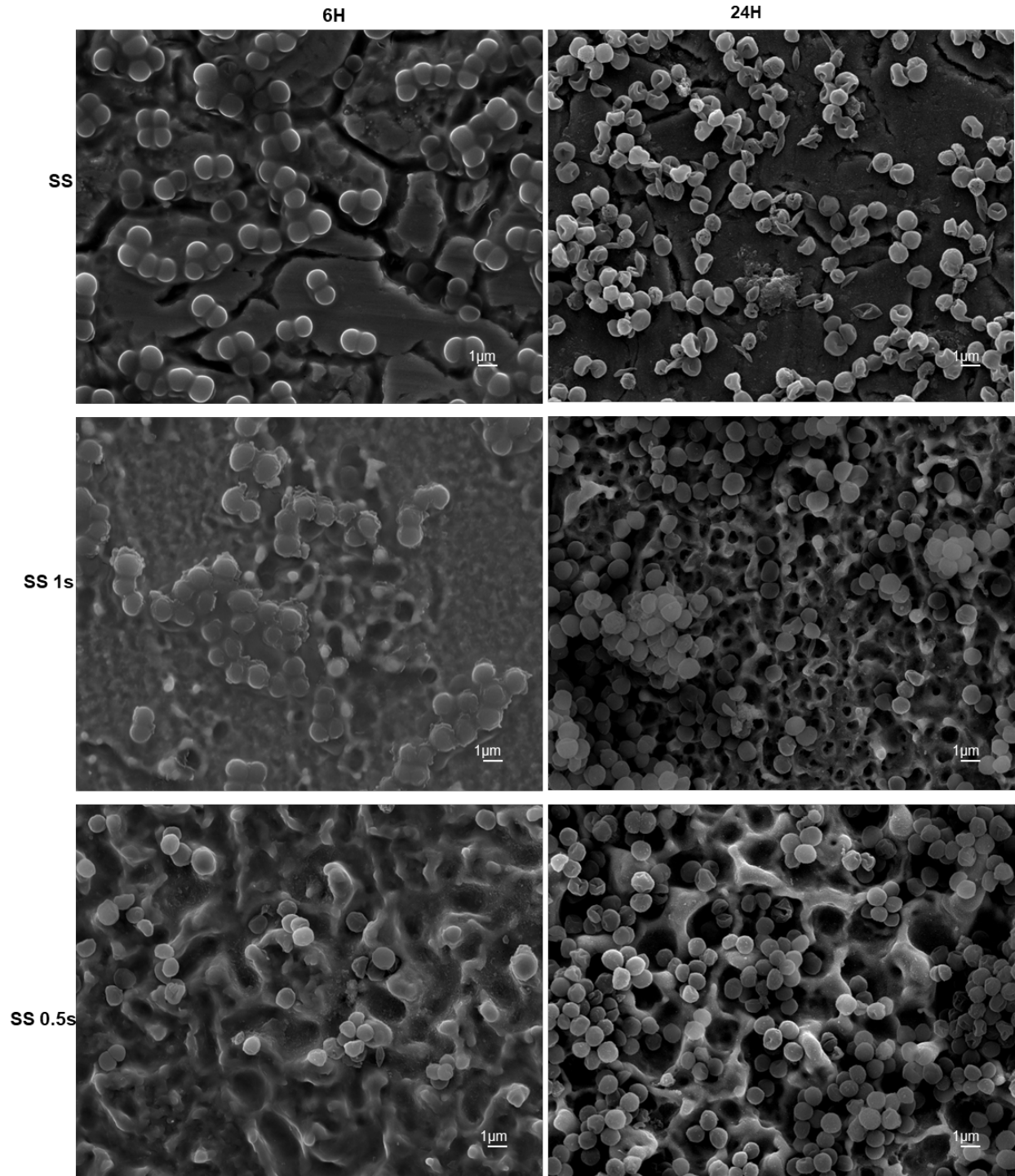
Figure 4.3.1 A) Representative fluorescence images of *S. aureus* on the different surfaces. *S. aureus* adhesion area percentage for live (B) and dead (C) bacteria after 6 and 24 hours. Significant differences of (***) indicates $p \leq 0.001$ for *S. aureus* coverage. Error bars represent the standard deviation.

4.3.2 Bacterial morphology

SEM images from *S. aureus* demonstrate similar findings for 6 & 24 hours as the results seen from fluorescence images (**Figure 4.3.2 A & B**). The PEO modified surfaces of SS 1s and SS 0.5s demonstrated less *S. aureus* adhesion at 6H when compared to SS. Upon further magnification at 5000x, the *S. aureus* bacteria has deformed at 24H for all surfaces. It can be seen at 24H on the SS surface that *S. aureus* has deposited materials on the surface that could lead to the formation of an increasing biofilm.



(A)



(B)

Figure 4.3.2 Representative SEM images of *S. aureus* on different surfaces at 1500x magnification. The red circles represent where the 5000x images were taken from the

1500x image. (A) Representative SEM images of *S. aureus* on different surfaces at 5,000x magnification (B).

Results from the live dead analysis showed a significant reduction, $p \leq 0.01$. in *S. aureus* for both live bacteria at 6 hours and dead bacteria at 24 hours surfaces SS 1s and SS 0.5s when compared to SS. It was demonstrated that *S. aureus* had deformed bacteria at the 24H period on all surfaces, while the SS surface deposits of material on the surface that could lead to biofilm formation. The differences seen between SS and the PEO modifies surfaces of SS 1s and SS 0.5s are attributable to the differences in surface morphology. As anti-biotic resistance increases the need for novel methods to prevent bacterial infections therein increases. By the SS 1s and SS 0.5s having a significant reduction in *S. aureus* adhesion the likelihood for an infection to occur on this material are vastly reduced. *S. aureus* infections tend to be opportunistic, as in the species desires optimal conditions, such as an invasive surgery for an implantable device. In fabricating materials that reduce bacterial adhesion as inherent property, the prevalence of implant failure will be reduced.

4.4 Conclusions

SS 1s and SS 0.5s showed a significant reduction in *S. aureus* adhesion when compared to SS. The morphology demonstrated that *S. aureus* had deposited materials onto the SS surface to begin biofilm formation. Together these findings demonstrate that the surface morphology fabricated by the PEO process was significant in reducing the adhesion and biofilm capability of *S. aureus* on to the surface.

REFERENCES

- [1] Sakka, S., Baroudi, K. and Nassani, M.Z. (2012), Factors associated with early and late failure of dental implants. *J Invest Clin Dent*, 3: 258-261. <https://doi.org.ezproxy2.library.colostate.edu/10.1111/j.2041-1626.2012.00162.x>
- [2] Urška Filipović, Raja Gošnak Dahmane, Slaheddine Ghannouchi, Anamarija Zore, Klemen Bohinc, Bacterial adhesion on orthopedic implants, *Advances in Colloid and Interface Science*, (2020), 283, 102228, <https://doi.org/10.1016/j.cis.2020.102228>.
- [3] Antonelli, Patrick J.*; Lee, James C.*; Burne, Robert A.†., Bacterial Biofilms May Contribute to Persistent Cochlear Implant Infection, *Otology & Neurotology*, (2004), 25, 6, 953-957, doi: 10.1097/00129492-200411000-00015.
- [4] Icggen, B. VanA-Type MRSA (VRSA) Emerged in Surface Waters, *Bull Environ Contam Toxicol*, (2016), 97, 359–366, <https://doi.org.ezproxy2.library.colostate.edu/10.1007/s00128-016-1827-2>
- [5] Kluytmans J, van Belkum A, Verbrugh H. Nasal carriage of *Staphylococcus aureus*: epidemiology, underlying mechanisms, and associated risks. *Clin Microbiol Rev.* (1997) Jul;10(3):505-20. doi: 10.1128/CMR.10.3.505.
- [6] Gordon Y. C. Cheung, Justin S. Bae & Michael Otto, Pathogenicity and virulence of *Staphylococcus aureus*, *Virulence*, (2021), 12:1, 547-569, DOI: 10.1080/21505594.2021.1878688

[7] Mohamed Hagra, Haroon Mohammad, Mohamed S. Mandour, Youssef A. Hegazy, Adel Ghiaty, Mohamed N. Seleem, and Abdelrahman S. Mayhoub, Investigating the Antibacterial Activity of Biphenylthiazoles against Methicillin- and Vancomycin-Resistant *Staphylococcus aureus* (MRSA and VRSA), *Journal of Medicinal Chemistry*, (2017), 60, 9, 4074-4085, DOI: 10.1021/acs.jmedchem.7b00392

[8] Jafar Hasan, Russell J. Crawford, Elena P. Ivanova, Antibacterial surfaces: the quest for a new generation of biomaterials, *Trends in Biotechnology*, (2013), 31, 5, 295-304, <https://doi.org/10.1016/j.tibtech.2013.01.017>.

CHAPTER 5

CONCLUSIONS AND FUTURE WORK

5.1 Conclusions

Orthopedic implants are biomaterials susceptible to failure. Two main sources of failure are due to adverse reactions caused by the innate and adaptive immune response, and bacterial infection.

316L stainless steel underwent surface modification using plasma electrolytic oxidation with pulse timings. The PEO parameters utilized a sodium bicarbonate solution with DC power at 120 V and 8 amperes for 1 second or 0.5 second intervals. The fabricated surfaces were characterized by their surface morphology, wettability, chemical composition, and crystallinity. The characterization of SS 1s and SS 0.5s yielded differences in the morphology & wettability; SS 1s and SS 0.5s were hydrophilic, 316L SS was slightly hydrophobic. While the surface chemistry and crystallinity remained similar to 316L SS.

Once characterization of the surfaces had been completed, the viability, adhesion, and osteointegration of adipocyte derived stem cells was investigated. ADSCs are mesenchymal cells with the ability to differentiate into osteoblasts when induced with specific cell culture media. The results from the fluorescence microscopy, an alamar blue cell viability assay, and scanning electron microscopy showed there were no significant

differences in the initial viability and adhesion of ADSCs at Days 1, 4, and 7 of the study between 316L SS, SS 1s, and SS 0.5s.

After the investigation into the cellular viability, adhesion, and osteointegration. The bacterial adhesion and morphology of the surfaces were characterized. *Staphylococcus aureus* was utilized in this investigation as it is a prevalent gram-positive nosocomial infection, that has known antibiotic resistant strains of MRSA and VRSA. After 6 hours of incubation, live *S. aureus* was seen to have a significant reduction in the adhesion on the PEO modified surfaces of SS 1s and SS 0.5s when compared to 316L SS. After 24 Hours of incubation, dead *S. aureus* was shown to have a significant reduction in the adhesion on the PEO modified surfaces of SS 1s and SS 0.5s when compared to 316L SS. Scanning electron microscopy found no biofilm formation on the PEO modified surfaces of SS 1s and SS 0.5s, and there some biofilm formation seen on 316L surfaces.

In conclusion, PEO modification was successful using pulse timings of 1 second and 0.5 seconds. The PEO modified surfaces were hydrophilic that maintained cellular adhesion, viability, and osteointegration. The PEO modified surfaces reduced the bacterial adhesion of *S. aureus* when compared to 316L SS. These findings suggest that PEO modification could be utilized on 316L stainless steel to fabricate a stable biomaterial that prevents bacterial infection.

5.2 Future Work

Future studies of this process include further investigation into how the surfaces interact with gram negative bacteria. An investigation *Pseudomonas aeruginosa* is a

bacterial species of interest as it is a prominent anti-biotic resistant nosocomial infection. It is relevant to understand how the surfaces interact with gram negative bacteria. Investigation into hemocompatibility of the surfaces will provide insights into how the surfaces would integrate with the human upon implantation, with the surfaces being hydrophilic the knowledge of blood platelet clotting is key for further development of this surface modification technique. Once the knowledge from *Pseudomonas aeruginosa* adhesion and hemocompatibility is known, of interest is use of using different PEO parameters such as different pulse timing, voltages, and amperages. Differences in how the DC power is supplied may affect how the PEO occurs on the surfaces, thus changing the surface topography and the surface wettability. Another investigation of interest is the repetition of these experiments with ion doped PEO surface with copper. The addition of copper would enhance the antibacterial capabilities of the surfaces, however the interaction with cells is desired knowledge.